Nuclear import of the DSCAM-cytoplasmic domain drives a signaling loop capable of inhibiting synapse formation

Sonja Sachse[1,2], Sam Lievens[3,4], Luís Ribeiro[1,2], Dan Dascenco[1,2], Katrien Horré[1,2], Anke Misbaer[1,2], Nele Vanderroost[3,4], Wouter Van Delm[5], Stéphane Plaisance[5], Jan Tavernier[3,4], Bart De Strooper[1,2,6], Joris DeWit[1,2], Dietmar Schmucker[1,2]

CORRESPONDING AUTHOR
Dietmar Schmucker
dietmar.schmucker@kuleuven.vib.be

1 VIB Center for Brain & Disease Research, Leuven, Belgium
2 KU Leuven, Department of Neurosciences, Leuven, Belgium
3 VIB Department of Medical Protein Research, Ghent, Belgium
4 Ghent University
5 VIB Nucleomics Core, Leuven, Belgium
6 Dementia Research Institute, University College London, UK

ABSTRACT

DSCAM and DSCAML1 are immunoglobulin and cell adhesion-type receptors serving important neurodevelopmental functions including control of axon growth, branching, neurite self-avoidance and neuronal cell death. The signal transduction mechanisms or effectors of DSCAM receptors however, remain poorly characterized. We used a human ORFeome library to perform a high-throughput screen in mammalian cells and identified novel cytoplasmic signaling effector candidates including the Down syndrome kinase Dyrk1a, STAT3, USP21, and SH2D2A. Unexpectedly, we further found that the intracellular domains (ICDs) of DSCAM and DSCAML1 specifically and directly interact with IPO5, a nuclear import protein of the beta-importin family, via a conserved nuclear localization signal. The DSCAM ICD is released by gamma-secretase dependent cleavage and both the DSCAM and DSCAML1 ICDs efficiently translocate to the nucleus. Furthermore, RNA-sequencing confirms that expression of the DSCAM as well as the DSCAML1 ICDs alone can profoundly alter the expression of genes associated with neuronal differentiation and apoptosis, as well as synapse formation and function. Gain-of-function experiments using primary cortical neurons show that increasing the levels of either the DSCAM or the DSCAML1 ICD leads to an impairment of neurite growth. Strikingly, increased expression of either full-length DSCAM or the DSCAM ICD, but not the DSCAML1 ICD, significantly decreases synapse numbers in primary hippocampal neurons. Taken together, we identified a novel membrane-to-nucleus signaling mechanism by which DSCAM receptors can alter the expression of regulators of neuronal differentiation, synapse

formation and function. Considering that chromosomal duplications lead to increased DSCAM expression in trisomy 21 our findings may uncover novel mechanisms contributing to mental retardation in Down Syndrome.

INTRODUCTION

The precise wiring of neuronal circuits as well as the establishment of synaptic specificity majorly relies on intracellular signaling pathways downstream of diverse families of cell surface receptors. Signaling of these receptors can be modulated by extracellular ligands, membrane associated molecular cues, and adhesive receptor-receptor interactions or combinations thereof. The Down syndrome cell adhesion molecule (DSCAM) receptors (Yamakawa et al., 1998) are important examples of receptors that utilize homophilic interactions during neurite growth, but can also interact with heterologous ligands (Dascenco et al. 2015). In vertebrates, there are two paralogous *DSCAM* genes, *DSCAM* and *DSCAML1* (*DSCAM-Like-1*) (Agarwala et al., 2001; Yamakawa et al., 1998). Human *DSCAM* is located in the so-called Down syndrome critical region (DSCR) on chromosome 21 and belongs thereby to a group of genes present in three copies in Down syndrome (DS) individuals (Yamakawa et al., 1998). Notably, DSCAM levels are increased in brains of DS patients and it has been speculated that this may contribute to the cognitive disabilities observed in DS (Bahn et al., 2002; Saito et al., 2000). DSCAM is also overexpressed in brain of DS mouse models (Alves-Sampaio et al., 2010; Amano et al., 2004), and in mice that overexpress Amyloid precursor protein (APP) (Jia et al., 2011), a causative gene in Alzheimer's disease. Dysregulated *Dscam* levels severely alter dendritic, axonal and synaptic development, which may explain how DSCAM gene-dosage imbalance could potentially contribute to the pathogenesis of neurological disorders. Overexpression of DSCAM in mice disrupts dendrite targeting and leads to increased neuronal cell death of retinal neurons (Li et al., 2015). Loss of DSCAM or DSCAML1 on the other hand results in increased neuron numbers, self-avoidance defects and disorganized layers in the retina (Fuerst et al., 2009; Fuerst et al., 2008), demonstrating that deregulated DSCAM levels result in altered neuronal apoptosis. Moreover, overexpression of DSCAM in cultured mouse cortical or hippocampal neurons significantly reduces outgrowth and branching of axons and dendrites (Alves-Sampaio et al., 2010; Jain and Welshhans, 2016). In *Drosophila*, expression of three Dscam1 copies *in vivo* alters synaptic transmission and synaptic plasticity at the neuromuscular junction leading to impaired locomotor coordination (Lowe et al., 2018) and causes synaptic targeting defects of sensory axons (Cvetkovska et al., 2013). Increased Dscam1 levels also lead to presynaptic arbor enlargement in developing fly sensory neurons (Kim et al., 2013; Sterne et al., 2015).

Drosophila Dscam1 has been studied most extensively because of its extraordinary molecular diversity generated by alternative splicing (Hattori et al., 2008; Kise and Schmucker, 2013; Schmucker et al., 2000; Sun et al., 2013). *Drosophila* Dscam1 is essential for key aspects of neuronal wiring including axonal growth, guidance, targeting, and branching (Chen et al., 2006; Dascenco et al., 2015; He et al., 2014; Hummel et al., 2003; Schmucker et al., 2000), dendritic field organization (Hughes et al., 2007; Matthews et al., 2007; Soba et al., 2007), and synaptic

connectivity (Millard et al., 2010). Although vertebrate *DSCAMs* lack extensive alternative splicing, many functions important for neuronal wiring are highly conserved from flies to mammals. Homophilic self-recognition of Dscams is required in flies and mice for neurite repulsion and self-avoidance of sister-neurites *in vivo* (Fuerst et al., 2008; Hattori et al., 2008; Hughes et al., 2007). *Dscams* also play conserved roles in establishing synaptic connectivity and specificity. In the developing mouse and chick retina, depletion of DSCAM *in vivo* disrupts layer specific targeting and synaptic connectivity of retinal interneurons (Fuerst et al., 2010; Yamagata and Sanes, 2008). In the mature mouse retina however, DSCAM is required for maintaining dendritic territories by inhibiting synaptic connectivity as well as axon and dendrite outgrowth of bipolar cells (Simmons et al., 2017). In *Aplysia* neurons, Dscam-mediated trans-synaptic interactions are required for the clustering of postsynaptic AMPA-like glutamate receptors and for synaptic transmission during de novo and learning related synaptogenesis (Li et al., 2009). Considering that DSCAM/L1 also bind to the postsynaptic scaffolding proteins MAGI and PSD95 (Yamagata and Sanes, 2010b), it suggests also a role for vertebrate DSCAM in synapse development and function.

Despite the conserved roles of Dscams in shaping neuronal circuitry, no coherent downstream signaling pathway has been identified. In the canonical model of axon guidance and synaptic receptor signaling, ligand binding results in recruitment of protein complexes to receptor intracellular domains thereby altering the dynamics of the actin- and tubulin-based cytoskeleton. *Drosophila* Dscam1 is thought to affect actin cytoskeleton dynamics through the SH2/SH3 adaptor protein Dock/Nck acting upstream of P21 activated kinase (Pak1) (Hing et al., 1999; Schmucker et al., 2000), which in turn interacts with Rho GTPases (i.e RhoA, Rac1, and Cdc42), regulators of actin cytoskeleton dynamics (Hall, 1998; Manser et al., 1994). However, loss of Dock or Pak1 does not lead to phenotypic defects such as dendrite self-crossing (Hughes et al. 2007) suggesting other effector molecules must exist. Dscam1 also physically and genetically interacts with tubulin folding cofactor D (TBCD), which is required for the formation of alpha- and beta–tubulin heterodimers in flies (Okumura et al., 2015). Vertebrate DSCAM has been implicated in the regulation of actin cytoskeleton dynamics during commissure axon guidance upon binding to the heterophilic ligand Netrin. DSCAM-Netrin interactions are thought to promote complex formation of DSCAM with the Netrin receptor UNC5C and the kinases PAK1, Fyn and FAK (Liu et al., 2009; Purohit et al., 2012), and to trigger the dissociation between DSCAM and the Netrin receptor DCC (Deleted in colorectal cancer) (Ly et al., 2008). But a loss-of-function analysis for testing the significance of these interactions *in vivo* has not been reported.

Here we identify several novel cytoplasmic signaling effectors of DSCAM/L1. We report that Importin 5 (IPO5) mediated membrane-to-nucleus translocation of DSCAM/L1 may provide a novel signaling mode of this important receptor class. We show that the ICD of mammalian DSCAM is liberated by γ-secretase-mediated cleavage and that both the DSCAM and DSCAML1 ICD efficiently translocate to the nucleus. Considering that increased DSCAM levels have been proposed to contribute to mental retardation in Down syndrome patients we tested in gain of function experiments how increased DSCAM signaling might affect neurite growth and synapse

formation. We show that nuclear enrichment of the DSCAM and DSCAML1 ICD in cell lines profoundly alters the transcription of genes associated with neuronal differentiation and function. Increased nuclear levels of either the DSCAM or DSCAML1 ICD, strongly impairs neurite outgrowth in primary mouse cortical cultures. Interestingly, only increased expression of either full-length DSCAM or the DSCAM ICD, but not of the DSCAML1 ICD, leads to a strong decrease in synapse numbers in primary mouse hippocampal neurons. Thus, these studies uncover how increased DSCAM membrane-to-nucleus signaling is capable of altering synaptic connectivity and suggest a novel scenario how gain of DSCAM function may contribute to neurological pathologies.

RESULTS

Identifying Human Signaling Effectors of DSCAM and DSCAML1

In order to identify novel cytoplasmic binding partners of vertebrate DSCAMs we employed the mammalian protein-protein interaction trap (MAPPIT) to monitor protein-protein interactions in mammalian cells (Figure 1A) (Eyckerman et al., 2001; Lievens et al., 2009). We generated MAPPIT receptors with the intracellular domains (ICDs) of mouse DSCAM or DSCAML1 serving as baits (Figure 1A) and performed high-throughput MAPPIT screens in which the DSCAM/L1 baits were screened against a library of about 10,000 preys (Lievens et al., 2011; Lievens et al., 2009). From these screens, we further selected and validated IPO5, DYRK1A, DYRK1B, SH2D2A, STAT3, and USP21 as binding partners of both DSCAM and DSCAML1 in binary MAPPIT experiments including control baits and preys (Table 1, Figure S1 A-B, Figure 1B, 1G). We also tested the interaction of the DSCAM and DSCAML1 (DSCAM/L1) bait receptors with preys of known binding partners including PAK1 (DSCAM) and MAGI-1 (DSCAM and DSCAML1) (Purohit et al., 2012; Yamagata and Sanes, 2010a). Both DSCAM and DSCAML1 baits gave rise to MAPPIT signals with MAGI-1 and the DSCAM bait also interacted with the PAK1 prey, but these interactions were weaker compared to newly identified candidates (Figure S1 C-D). Recruitment of kinases and SH2-domain adaptor proteins were expected based on previous studies on *Drosophila* Dscam1 (Schmucker et al. 2000); however, neither DYRK1A (also referred to as "Down Syndrome kinase") nor SH2D2A have been previously implicated in DSCAM signaling.

Using the Eukaryotic Linear Motif (ELM) platform and published information (Tinti et al., 2013), we further validated the results of the MAPPIT screen by identifying specific tyrosine residues in the DSCAM/L1 ICDs predicted to serve as binding motifs for the SH2-domains of STAT3 (YxxQ motif) and SH2D2A (YxNL motif). DSCAM possesses one highly conserved YxxQ motif, whereas DSCAML1 exhibits two YxxQ motifs (Figure S2 A) as well as one YxNL motif (Figure S2 F). Mutations of those tyrosine residues to phenylalanine in the bait receptors abolished the interactions of DSCAML1 with STAT3 and SH2D2A as well as between DSCAM and STAT3 in

MAPPIT assays, whereas the interaction with the IPO5 prey was not affected, suggesting that the identified tyrosine motifs are the binding sites for the SH2 domains of STAT3 and SH2D2A (Figure S2 B, D, and G). DSCAM does not have an YxNL/SH2D2A consensus motif and single mutations of the 9 tyrosine residues present in the DSCAM cytoplasmic tail could not abolish the interaction between DSCAM baits and SH2D2A (Figure S2 H), suggesting that the interaction might not depend on the recognition of a single tyrosine residue by the SH2 domain of SH2D2A. Surprisingly, mutation of the identified YxxQ/STAT3 consensus motifs in DSCAM/L1 bait receptors also significantly reduced the interaction with USP21 (Figure S2 B and D), indicating that USP21 either binds to the YxxQ motifs or interacts with STAT3. For clarification we would like to note that DSCAM/L1 bait receptors gave rise to background signals in binary MAPPIT experiments, i.e. generating a signal in the absence of an interaction (Figure S2 C, E). This can be explained by activation of endogenous STAT3 signaling upon binding to the DSCAM/L1 bait receptors. Consistently, the STAT3 binding deficient mutant DSCAM (i.e. LR-DSCAM^{Y1746F}) and DSCAML (i.e. LR-DSCAML1$^{Y1744F/\ Y1937F}$) baits did not generate background signals and were therefore used in follow up binding experiments as indicated (Figure S2 C, E).

DYRK1A and *DYRK1B* are paralogous genes of the dual-specificity tyrosine-regulated kinase (DYRK) family (Becker et al., 1998; Leder et al., 1999). A DYRK1B prey consisting of the most C-terminal 72 amino acids and lacking the kinase domain was present in the MAPPIT library (Figure 1C). The truncated DYRK1B prey interacted with DSCAM and DSCAML1 baits in MAPPIT, generating a signal comparable to a full length DYRK1B prey (Figure 1D, Figure S3 A), demonstrating that the kinase domain of DYRK1B is not required for the interaction with DSCAMs. Furthermore, a truncated DYRK1A prey consisting of its N-terminal and its kinase domains but lacking its C-terminal domains (Figure 1C) failed to bind to the DSCAM or DSCAML1 baits in contrast to full-length (FL) DYRK1A (Figure 1E, Figure S3 B). Both DSCAM and DSCAML1 ICDs exhibit a potential DYRK substrate motif (RPGTNP). A triple alanine substitution of the RPx(T/S/x)P motif was previously shown to be sufficient to abolish the interaction of DYRK1A with a substrate peptide (Soundararajan et al., 2013). Thus, we generated triple alanine substitution mutant baits (RPGTNP to AAGANP) for both DSCAM and DSCAML1 and tested binding to DYRK1A and DYRK1B preys in MAPPIT. However, the AAGANP mutant baits could still interact with DYRKs (Figure 1F, Figure S3 C-D), suggesting that binding of DYRKs to DSCAMs might be independent of their kinase domains, as previously shown for other DYRK1A interactors (Aranda et al., 2008). In conclusion, the MAPPIT approach lead to the identification of IPO5, STAT3, DYRK1A/B, SH2D2A, and USP21 as novel potential downstream effectors of DSCAM.

DSCAMs Interact with IPO5 via a Nuclear Localization Signal

Since binary MAPPIT assays revealed strong interactions of both DSCAM and DSCAML1 with Importin 5 (IPO5) (Figure 1G), we reasoned that DSCAMs might have nuclear

functions. Such membrane to nucleus signaling mechanism would be similar to Neogenin and DCC, two neuronal CAMs that are closely related to vertebrate DSCAMs and cleaved by proteases resulting in the release of C-terminal ICD fragments, which then translocate into the nucleus where they regulate gene transcription (Goldschneider et al., 2008; Taniguchi et al., 2003). IPO5 is a beta importin mediating nuclear protein import (Yaseen and Blobel, 1997) and can directly interact with the nuclear localization signal (NLS) of its cargo (Chao et al., 2012b). We therefore considered that the ICDs of DSCAMs might contain an NLS serving as docking site for IPO5. Indeed, upon sequence analysis we identified a monopartite NLS within the membrane proximal regions enriched in conserved Arginine and Lysine residues (Figure 1H). Interestingly, *Drosophila* Dscam1 also exhibits a predicted NLS within the cytoplasmic portion that is common to all its isoforms, indicating that a membrane-proximal NLS is highly conserved from insects to vertebrates (Figure 1H). To test its functional relevance, we generated NLS-deficient MAPPIT bait versions (i.e. LR-DSCAM$^{\Delta NLS}$ and LR-DSCAML1$^{\Delta NLS}$), which failed to interact with the IPO5 prey but could still interact with the STAT3 control prey (Figure 1I), demonstrating that the NLSs are required for the interaction between IPO5 and DSCAMs. To determine specificity, we tested all full-length alpha and beta importin preys present in the human ORFeome collection 5.1 and 8.1. Out of the 9 importins tested, only IPO5 interacted with DSCAM and DSCAML1 (Figure 1J). Together, these results show that IPO5 can bind to the membrane proximal NLS motifs of DSCAMs with high specificity.

DSCAM is cleaved by γ-secretase

Several neuronal transmembrane proteins including APP, DCC, Neogenin and Notch undergo ectodomain cleavage directly followed by γ-secretase mediated intra-membrane cleavage leading to the release of their ICDs (De Strooper et al, Nature 1999, , Cupers et al 2001, Cao and Sudhof, 2001; Goldschneider et al., 2008; Taniguchi et al., 2003). Shedding of the DSCAM ectodomain has been reported in flies and mice (Schramm et al., 2012; Watson et al., 2005), however it is currently unknown whether the ICD of DSCAMs could be released by proteolytic cleavage. To investigate this, we fused HA-epitopes to the very C-terminus of the DSCAM/L1 ICDs as well as to FL DSCAMs (Figure 2A) and expressed these fusion proteins in HEK293T cells. Immuno-precipitation with an HA-specific antibody and Western Blot (WB) analysis showed FL DSCAM migrating at approximately 250 kDA as well as a C-terminal fragment at 55 kDa, which co-migrates with the DSCAM ICD construct at approximately the same molecular weight (Figure 2B). Likewise, FL DSCAML1 migrated at nearly 250 kDa and we detected two additional C-terminal fragments migrating at 65 kDa and at 60 kDa, co-migrating with two fragments originating from the DSCAML1 ICD HA-fusion (Figure 2B). This suggests that DSCAMs are substrates for a protease and cleavage generates C-terminal ICD fragments.

We further employed a cleavage luciferase reporter assay in which DSCAM and DSCAML1 were C-terminally fused to a Gal4DBD–VP16 transactivation domain (TAD) (Karlstrom et al., 2002; May et al., 2002). Cleavage of these constructs releases the Gal4DBD–VP16 fusion protein fragment, which can transcriptionally activate a co-transfected luciferase

gene (Figure 2C). As compared to control cells expressing a non-cleavable IFNaR1-Gal4DBD-VP16 receptor, cells expressing the DSCAM or DSCAML1 fusion proteins showed a strong increase in luciferase activity similar to cells expressing a constitutively cleaved (IFNaR2-Gal4bd-VP16) or a constitutively active control (Gal4bd-VP16-empty) (Figure 2D). These data confirm that the ICDs of DSCAMs can be released upon proteolytic cleavage and that likely the entire ICD is shuttled to the nucleus.

We also investigated a potential *in vivo* cleavage of *Drosophila* Dscam1. In brain lysates of wild-type (wt) as well as flies harboring a BAC-based genomic transgene where the full-length Dscam1 gene is HA-tagged in exon 22 (i.e. cytoplasmic domain; see Supplementary Methods) we detected FL Dscam1 at 250 kDa and an additional band at 55kDa, while these bands were absent in control lysates from WT flies. Using a previously validated antibody directed against the ICD of fly Dscam1 ICD (Watson et al., 2005) we also detected FL Dscam1 as well as a 55kDa fragment in WT samples (Figure 2E), suggesting that endogenous Dscam1 is cleaved as well. This suggests that *Drosophila* Dscam1 is processed by proteolysis *in vivo* and that the cleavage of DSCAM family IgCAMs is conserved from vertebrates to flies.

To determine whether vertebrate DSCAM is a substrate of γ-secretase we treated HEK cells stably expressing C-terminally HA-tagged DSCAM with or without the proteasome inhibitor Lactacystin in the presence or absence of two different γ-secretase inhibitors (DAPT and Inhibitor X). Lactacystin was added to stabilize intracellular fragments generated by γ-secretase as these are rapidly degraded by proteasome (Cupers et al., 2001) WB analysis of lysates in the presence of Lactacystin and in the absence of Inhibitor X or DAPT revealed a stabilized fragment of about 50 kDa. This fragment was absent in the presence of either Inhibitor X or DAPT, and instead a prominent higher-molecular-mass fragment of 55 kDa was detected (Figure 2F). Taken together, this suggests that DSCAM is a novel γ-secretase substrate and its cleavage releases a 50 kDa “γ-product” (Figures 2F-G).

The ICDs of DSCAM and DSCAML1 Translocate into the Nucleus

The predicted NLS motif in DSCAM as well as DSCAML1 is highly conserved in vertebrates (Figure 3A) where an Arginine- or Lysine-rich eight amino acid peptide in DSCAM or DSCAML1, respectively, is followed by an invariant 20 amino acid sequence. Moreover, DSCAM or DSCAML1 interactions with the nuclear import factor IPO5 are eliminated when the putative NLS motifs are missing in MAPPIT baits (Figure 1I). To further validate that these conserved NLS motifs are indeed necessary for nuclear import of the DSCAM/L1 ICDs, we added C-terminal YFP-tags to wt and NLS-deficient protein forms (Figure 3A). We expressed these YFP-tagged constructs in HEK293T cells and analyzed their sub-cellular localization. Both wt DSCAM and DSCAML1 ICD were predominantly located in the nucleus (Figure 3B), whereas in cells expressing the NLS-deficient ICDs YFP fluorescence was absent from the nucleus but present throughout the cytoplasm or in perinuclear compartments (Figure 3C). On the other hand, FL YFP-tagged DSCAM and DSCAML1 were enriched at the membrane between cell-cell contacts and also present in the cytoplasm, yet undetectable in the nucleus (Figure 3D). This

suggests that in HEK cells, where DSCAM and DSCAML1 are not endogenously expressed, cleavage of full-length proteins is scarce. This however is different in developing cortical neurons (see below), which endogenously express both DSCAM and DSCAML1 (Barlow et al., 2002; Cui et al., 2013). We used nucleofection of E14.5 cortical neurons and analyzed subcellular localization of the same YFP-tagged proteins (Figure 3A) after 4 days *in vitro* (DIV4). The YFP-tagged ICDs, similarly to our findings in HEK cells, were enriched in the nucleus of cortical neurons (Figure 3E), whereas the NLS-deficient ICDs were predominantly localized in the cytoplasm of cell bodies and neurites (Figure 3F). In line with their function as neuronal CAMs, FL DSCAM/L1 YFP-fusions were localized at the neuronal membrane and enriched at neurite-neurite contacts (Figure 3G). Strikingly, in neurons expressing YFP-tagged FL DSCAM/L1 we also detected substantial YFP-signal in the nucleus (Figure 3G) most likely resulting from cleavage of DSCAM receptors. Hence, there is a striking difference between HEK cells and primary neurons, suggesting that cleavage or nuclear import of DSCAM is facilitated in neurons. Taken together, our results show that in mammalian neurons, overexpression of DSCAM/L1 leads to significant proteolytic cleavage of FL receptors and that a conserved membrane-proximal NLS motif is essential for translocation of the entire ICD to the nucleus.

Nuclear Localization of the DSCAM/L1 ICDs Alters the Expression of Genes Involved in Neuronal Wiring

Cleavage and nuclear import has been described for a number of membrane receptors yet this mechanism has previously not been implicated in DSCAM signaling. We therefore investigated the possibility that nuclear translocation of the DSCAM/L1 ICDs could substantially alter gene transcription. To test this, we stably expressed the YFP-tagged DSCAM and DSCAML1 ICDs as well as cytoplasmic and nuclear YFP controls in HEK293 t-Rex-Flp-In cells and subsequently performed RNA deep sequencing (RNA-Seq). We used the HEK293 t-Rex-Flp-In expression system because it offers stable and uniform expression of transgenes from a defined genomic locus, and because expression is inducible, two features which are not possible to achieve in primary neuron cultures. We then determined the global transcriptome changes of cells expressing the YFP-tagged DSCAM/L1 ICDs versus cells expressing a nuclear YFP as control (Figure 4A). We stringently excluded from our analysis genes that were already differentially expressed in cytoplasmic versus nuclear YFP expressing cells (p- value ≤ 0.1), as these genes are unlikely affected by DSCAM ICD expression (Figure 4A). Notably, choosing this stringent cut-off may have led to the elimination of some positive candidate DEGs, which, however, may be relevant candidates rather than false positives. Statistical analysis (p-value ≤ 0.0005; log ratio ≥0.58, ≤ -0.58) revealed a total of 1028 differentially expressed genes (DEGs) in response to DSCAM-ICD-expression (i.e. DSCAM data set; 434 down-regulated, 648 up-regulated; Figure 4B, S4A) and 860 DEGs in response to DSCAML1-ICD-expression (i.e. DSCAML1 data set; 328 down-regulated, 532 up-regulated; Figure 4B, S4B), with 552 DEGs that are in common to the two data sets (Figure 4C). Despite the use of non-neuronal cells, the functional

categorization of those DEGs using Ingenuity Pathway Analysis (IPA) identified “nervous system development and function” as a statistically highly enriched biological function ($p < 0.005$) and “axonal guidance signaling” as the most enriched canonical pathway ($p = 2.45E-05$) in both data sets (Figure S4C-D, table S2-3) encompassing about 240 DEGs for DSCAM and 190 DEGs for DSCAML1 altogether. To illustrate the remarkable enrichment for neuronal differentiation genes, we narrowed the DSCAM and DSCAML1 data sets down to about 90 candidate genes based on their well-known functions in axon guidance, neurite repulsion, branching, synaptogenesis and neuronal cell death (Figure 4D and 4E). For simplicity, they are further grouped based on subcellular localization (membrane, cytoplasmic, extracellular, and nuclear) (Figure 4D and 4E).

Several receptors and ligands involved in repulsion, axon guidance, and branching were up-regulated in both the DSCAM and DSCAML1 datasets; for example, Robo2 (Roundabout Guidance Receptor 2), UNC5A (Unc-5 Netrin Receptor A), PLXNC1 (Plexin C1), NTN4 (Netrin 4), and NTNG2 (Netrin G2) (Figure 4D and 4E). Specific to the DSCAM data set a cluster of Ephrins, namely EFNA3 (Ephrin A3), EFNA4 (Ephrin A4), EFNB3 (Ephrin B3), as well as SEMA3E (Semaphorin 3E), and RGMA (Repulsive Guidance Molecule Family Member A) were also up-regulated (Figure 4D and 4E). Thus, overexpression of DSCAM/L1-ICDs leads to a specific up-regulation of several key players involved in neurite repulsion, suggesting that transcriptional regulation via membrane to nucleus signaling of DSCAMs might play a role in mediating their repulsive functions during neuronal circuit formation.

DSCAM was also shown to regulate microtubule dynamics through interactions with TUBB3 during Netrin-1-induced axonal branching (Huang et al., 2015). Strikingly, several structural components of the tubulin cytoskeleton and neuronal intermediate filaments were down-regulated in the DSCAM and DSCAML1 datasets, including the neuron-specific tubulin TUBB3 (Tubulin Beta 3 Class III), as well as TUBA4A (Tubulin Alpha 4A), TUBB2A (Tubulin Beta 2A Class IIA, only DSCAML1), and NEFH (Neurofilament Heavy). Moreover, the microtubule cytoskeleton regulators MAPT (Microtubule Associated Protein Tau) and MAP2 (Microtubule Associated Protein 2) were up-regulated in the DSCAM and DSCAML1 datasets (Figure 4D and 4E). Taken together, this indicates that DSCAMs may, in addition to direct interactions with tubulin, affect neuronal cytoskeletal dynamics by regulating the expression of tubulins, crucial microtubule regulators, as well as neurofilaments.

Several proteins involved in neurotrophic signaling were also up-regulated, including the BDNF receptor NTRK2 (neurotrophic tyrosine kinase receptor 2, TrkB), NTF3 (neurotrophin 3, DSCAM only), the Trk-related receptor tyrosine kinase ROR2 (Receptor Tyrosine Kinase Like Orphan Receptor 2, DSCAM only) and BDNF-AS (Brain Derived Neurotrophic Factor Antisense RNA). Neurotrophic factors and their respective receptors, the Trk family of receptor tyrosine kinases (i.e. TrkA, TrkB, TrkC, and p75NTR), are key regulators of neural cell death and survival (Lu et al., 2005), and also have important functions in neurite branching and differentiation, as well as synapse formation, maturation, and function (Park and Poo, 2013). Notably, both DSCAM and DSCAML1 have been reported to have pro-apoptotic functions

during retinal development but the molecular mechanisms are not known (Fuerst et al., 2009; Fuerst et al., 2008; Li et al., 2015). Taken together, our transcriptome analysis shows that nuclear enrichment of the DSCAM and DSCAML1 ICDs triggers transcriptional changes of genes involved in neurite repulsion, axon guidance, branching, synapse formation and neuronal cell death.

Nuclear DSCAM and DSCAML1 Impair Neurite Outgrowth

Since our transcriptome analysis suggests that over-expression of DSCAM/L1 ICDs alters the expression of genes involved in neuronal differentiation and synapse formation, we next investigated the role of these ICDs in primary neurons. It has been shown that overexpression of full-length DSCAM in cortical pyramidal neurons significantly inhibits axon growth and branching in a dosage-dependent manner (Jain and Welshhans, 2016). Furthermore, DSCAM overexpression in mouse hippocampal neurons inhibits dendritic branching and leads to a reduction of total dendrite length (Alves-Sampaio et al., 2010). In order to test whether a membrane to nucleus signaling loop might contribute to the regulation of neurite growth we first transduced low-density cortical cultures at DIV1 with lentiviral constructs expressing YFP-tagged wt and NLS-deficient DSCAM/L1 ICDs, as well as a nuclear YPF-control (see Figure 3A). We immuno-stained the cultures for neuron-specific tubulin (Tuj1) at DIV4 and subsequently traced the tubulin cytoskeleton from randomly selected single YFP-positive neurons (see Methods). Nuclear localization of the DSCAM or DSCAML1 ICDs resulted in a significant reduction of total neurite length as compared to controls with YFP expression (DSCAM, 39 % shorter; DSCAML1 47 % shorter) or NLS-deficient ICDs (DSCAM, 44 % shorter; DSCAML1, 44% shorter) (Figure 5A-C). Moreover, we observed a significant decrease of the length of the longest neurite in neurons expressing the DSCAM ICD (49 % shorter) or DSCAML1 ICDs (48 % shorter) (Figure 5B-C). Notably, we did not observe significant differences in total neurite length or length of the longest neurite when comparing cultures expressing the YFP control and the NLS-deficient ICDs (Figure 5A-C). Taken together this demonstrates that enhanced nuclear translocation of the DSCAM and DSCAML1 ICDs profoundly impairs neurite outgrowth and development of primary cortical neurons.

Increased Nuclear DSCAM Levels Inhibit Synapse Formation

The DSCAM/L1 transcriptome data sets also contained a significant number of genes known to regulate synapse formation or function. Yet a role of mammalian DSCAM at the synapse or during synapse development has not been investigated directly. This may in part be due to the fact that early neurodevelopmental defects in DSCAM mutant mice likely mask later

roles at synapses. We therefore set out to test whether nuclear translocation of the DSCAM/L1 ICDs could affect synapse density in developing neurons. We quantified excitatory synapse density in primary mouse hippocampal cultures electroporated at E18 with wt and NLS-deficient YFP-fusions of the DSCAM/L1 ICDs, YFP-tagged full-length DSCAM/L1, and a nuclear YPF control plasmid. At DIV10 we determined the density of excitatory synapses defined as puncta double-positive for the post-synaptic marker PSD95 and the pre-synaptic marker Vglut1 normalized over dendrite length as described previously (Ko et al., 2009; Savas et al., 2015). Expression of full-length DSCAM or of the DSCAM ICD strongly and significantly decreased synapse density as compared to control cultures expressing YFP or the NLS-deficient mutant. This reduction of synapse density was characterized by a decrease in puncta positive for both PSD95 and Vglut1 (Figure 6A-D and S6A). This suggests that nuclear enrichment of the DSCAM ICD is sufficient to recapitulate the effect of full length DSCAM on synapse density.

We also examined the potential cell non-autonomy of defects in synapse formation in DIV10 hippocampal cultures electroporated with the DSCAM ICD (Figure 6E). Strikingly, in cultures electroporated with the DSCAM ICD, neighboring non-transfected neurons also exhibited significantly reduced synapse density characterized by a reduction of both PSD95 and VGlut1 puncta (Figure 6F-G and S6B-D). However, this cell non-autonomous effect on synapse density was weaker as compared to neurons transfected with the DSCAM ICD (Figure 6G). We therefor conclude that nuclear translocation of the DSCAM ICD has a cell autonomous and a cell non-autonomous effect on the development of synapses in hippocampal neurons. A cell non-autonomous function would be consistent with the scenario that a DSCAM ICD dependent nuclear signaling loop alters expression and levels of (likely secreted) factors that inhibit synapse formation in neighboring neurons.

We further observed that in primary DIV10 hippocampal neurons full-length DSCAM and DSCAML1 expression resulted in a different pattern of subcellular localization. While for DSCAM a substantial nuclear localization was apparent, DSCAML1 was predominantly located at the cell membrane (Figures 6H-I). Moreover, expression of full-length DSCAML1 in hippocampal neurons resulted in only a slight reduction of synapse density as compared to YFP-expressing control cultures, and expression of the DSCAML1 ICD alone did not have an effect on synapse density (Figures 6J-M and S7). The small effect of full-length DSCAML1 on synapse formation in contrast likely does not depend on a nuclear feedback loop in line with the distinct subcellular distribution we observed for DSCAM and DSCAML1 in these neurons. Taken together, this suggests that the effect of full-length DSCAM on synapse formation in hippocampal neurons depends to a significant degree on cleavage and nuclear translocation of its ICD.

DISCUSSION

Novel membrane-to-nucleus signaling of DSCAMs

Previous studies emphasized the importance of local cytoskeletal regulation as the central modus of DSCAM-dependent signaling (Huang et al., 2015; Liu et al., 2009; Okumura et al., 2015; Purohit et al., 2012; Schmucker et al., 2000). Several findings presented in this study, however, reveal a previously overlooked yet potentially conserved membrane to nucleus signaling mechanism of DSCAM receptors. The top candidates of our newly identified DSCAM/L1 binding partners are IPO5, STAT3, SH2D2A, DYRK1A, DYRK1B, USP21. All of these factors show a surprisingly close link to nuclear functions. The most prominent one being the transcription factor STAT3. It is well known that STAT3 dimers directly bind to DNA and get activated downstream of cytokine receptors, through phosphorylation by receptor tyrosine kinases such as the epidermal growth factor receptor (EGFR), and non-receptor tyrosine kinases like Src kinases (David et al., 1996; Reich and Liu, 2006). Moreover, the kinase DYRK1A can get recruited to promoters of genes actively transcribed by RNAPII, where it phosphorylates RNAPII, thereby activating gene transcription (Di Vona et al., 2015). But also DYRK1B, SH2D2A and USP21 have been shown to be involved in transcriptional regulation (Lim et al., 2002; Marti et al., 2006; Nakagawa et al., 2008).

These findings together with our studies on proteolytic processing and nuclear import of DSCAM suggest a potentially important membrane to nucleus signaling mechanism of DSCAM receptors. Such a mechanism resembles for example the signaling mode of the Notch receptor (Bray, 2006). Ligand binding to Notch (i.e Jagged and Delta) promotes shedding of the Notch ectodomain by ADAM-family metalloproteases, followed by a second intra-membrane cleavage mediated by the gamma-secretase complex (Bray, 2006). The second cleavage releases the Notch intracellular domain (Nicd), which in turn translocates to the nucleus where it acts as transcriptional co-factor to modulate gene expression of Notch target genes (Bray, 2006).

While Schramm and colleagues previously reported shedding of the DSCAM ectodomain (Schramm et al., 2012), and ectodomain cleavage has also been shown for *Drosophila* Dscam1 (Watson et al., 2005), the shedding protease of DSCAM receptors has not yet been identified. tIn any event, the reported cleavage product leaves an ectodomain stub, which serves as gamma-secretase substrate. In the case of Notch, metalloprotease cleavage depends on ligand binding, whereas subsequent intra-membrane cleavage by gamma-secretase is constitutive (Struhl and Adachi, 2000). This raises the question of whether cleavage and subsequent nuclear localization of the DSCAM/L1 ICDs might be ligand dependent. However, we observed gamma-secretase cleavage of DSCAM in the absence of ligand-treatment in cell cultures. Thus it is possible that also extracellular factors alone or in combination with homophilic DSCAM interactions in cis or trans may regulate DSCAM cleavage.

Functions of DSCAM-dependent Membrane to Nucleus Signaling in Neural Development

Accumulating evidence supports the concept that specific aspects of neuronal morphogenesis may be controlled by dynamic transcriptional feedback programs in response to

transmembrane receptor signaling at growth cones or synapses (Bao et al., 2004; Neuhaus-Follini and Bashaw, 2015; Yang et al., 2009). For example, the axon guidance receptor Frazzeled (Fra), which is the *Drosophila* homologue of DCC and expressed in neuronal growth cones, was shown to be cleaved by γ-secretase releasing its intracellular domain (Neuhaus-Follini and Bashaw, 2015). The Fra ICD translocates into the nucleus where it functions as a transcriptional activator regulating the expression of commissureless *in vivo* (Neuhaus-Follini and Bashaw, 2015; Yang et al., 2009). Commissureless on the other hand is a factor controlling midline crossing by negatively regulating the amount of repulsive Robo receptors at the cell surface of pre-crossing commissural axons (Neuhaus-Follini and Bashaw, 2015; Yang et al., 2009). Thus, it is tempting to speculate that a potential transcriptional regulation mediated by DSCAM receptors might serve to selectively regulate the responsiveness of neurons to repulsive axon guidance and/or death and survival promoting cues and thereby contribute to the spatial, temporal and cell-type-specific fine-tuning of neural circuit assembly. Importantly, the surprisingly strong impact of the DSCAM ICD on synapse formation and the observed non-autonomous inhibition of synapse formation are certainly consistent with a DSCAM-dependent retrograde signaling via nuclear import.

DSCAM and DSCAML1 specifically interacted with the beta-importin IPO5, whereas deletion of the identified NLSs abolished this specific interaction and suppressed nuclear translocation of the DSCAM/L1 ICDs in cell lines and cultured neurons. This suggests a direct role of IPO5 in the nuclear import of the DSCAM/L1 ICDs. Nuclear protein import can be accomplished by a complex consisting of an alpha- and a beta-importin or by beta-importins acting alone (Freitas and Cunha, 2009; Xu et al., 2010). IPO5 was shown to interact directly with the NLS of the cytoplasmic polyadenylation element-binding protein (CPEB) 3, mediating its NMDA-induced nuclear translocation in neurons (Chao et al., 2012a). Considering that we tested five out of seven human alpha importins (Miyamoto et al., 2016) and none of them interacted with DSCAMs, it seems also possible that IPO5 binds directly to DSCAMs without involvement of an alpha importin.

Even though intra-membrane cleavage and nuclear translocation has been shown for several neuronal receptors (Goldschneider et al., 2008; Kopan et al., 1996; Neuhaus-Follini and Bashaw, 2015; Taniguchi et al., 2003), very little is known about the molecular mechanisms of their nuclear translocation from distant axon terminals or synapses. A study in Drosophila showed that nuclear import of the C-terminus of the Wnt receptor Frizzled2 requires importins to promote postsynaptic development (Mosca and Schwarz, 2010). Importins are localized in dendrites, axons and synapses (Hanz et al., 2003; Mosca and Schwarz, 2010; Perry et al., 2012; Thompson et al., 2004) and their molecular interactions and subcellular localization at synapses can be altered by neuronal activity during neuronal plasticity (Jeffrey et al., 2009; Thompson et al., 2004). Furthermore, importins are involved in synapse-to nucleus transport as well as nuclear import of synaptic proteins (Lever et al., 2015; Panayotis et al., 2015), and have been reported to enable retrograde signaling in regenerating axons after injury (Hanz et al., 2003; Perry et al., 2012). Our data indicate that importin-mediated membrane-to-nucleus

signaling may also play a role in neurite and synapse development downstream of DSCAMs. Taken together, we speculate that importin-mediated membrane to nucleus communication from distant growth cones and synapses may represent a more general attribute of neuronal receptor signaling.

Potential gain of function effects of DSCAM by gene dosage increase in trisomy 21

Interestingly, mouse models of Down Syndrome (e.g. Ts1Cje) as well as studies on DS patients reveal abnormal patterns of gene expression in the brain during embryonic development and adulthood (Guedj et al., 2015a; Guedj et al., 2015b). These studies suggest that overexpression of certain proteins in DS brains may cause long-term transcriptional changes during brain development. Interestingly, in addition to DSCAM also Dyrk1a is located in the DS critical region (Shindoh et al., 1996; Yamakawa et al., 1998) and overexpressed in DS patients (Liu et al., 2008; Saito et al., 2000). It seems therefore possible that co-expression of these three signaling factors may lead to a synergistic enhancement of this signaling unit. Therefore, investigating these potentially deleterious gain-of-function effects and in particular the transcriptional alterations in response to activity of the DSCAM ICD may greatly increase our understanding of the molecular mechanisms that contribute to the emergence of neurodevelopmental disorders in mental retardation associated with Down Syndrome.

EXPERIMENTAL PROCEDURES

Additional details are provided in online Supplemental Experimental Procedures.

MAPPIT

MAPPIT screens were performed as described previously (Lievens et al., 2009) (Simicek et al., 2013). The prey collection screened consisted of a subset of 9.870 human ORF preys selected from the human ORFeome collection version 5.1 (http://horfdb.dfci.harvard.edu/hv5/).

Neuronal Cultures and Transfections

Low-density neuronal cultures were established as described in (Kaech and Banker, 2006). In brief, neurons were cultured from E14-15 cortices or E17-18 hippocampi of C57BL/6J mice and plated on poly-D-lysine (Millipore) and laminin (Invitrogen) coated glass coverslips (Marienfeld GmbH) and grown on top of a glial feeder layer. Neurons were maintained in Neurobasal medium (Invitrogen) supplemented with B27, glucose, glutamax, penicillin/streptomycin (Invitrogen), 20 mg/ml insulin (Sigma), and 25 mM b-mercaptoethanol. Hippocampal neurons were electroporated with plasmid DNA just before plating with the mouse neuron AMAXA Nucleofectorkit (Lonza) and immuno-stained at 10 days in vitro (DIV10). Lentiviral infections of cortical neurons were performed at DIV1 and neuronal morphology was analyzed at DIV4.

Image Acquisition and Analysis

Images were taken with a Zeiss LSM710 confocal microscope using a 40X/1.2NA water immersion or a 20x/0.8NA objective (Zeiss, Jena, Germany). Confocal images were processed by the use of the Fiji (Schindelin et al., 2012) software. Analysis of neurite length was performed on YFP-positive neurons using the skeletonize/analyze skeleton and simple neurite tracer plugins in Fiji. Analysis of synaptic density was performed on transfected YFP-positive neurons as described in (Savas et al., 2015).

RNA Sequencing

Libraries were prepared from RNA of three 3 biologically independent experiments. Sequence-libraries of each sample were equimolarly pooled and sequenced on an Illumina NextSeq 500 instrument (High Output, 75 bp, Single Reads, v2) at the VIB Nucleomics core (www.nucleomics.be). Differentially expressed genes were uploaded into the IPA software (Ingenuity Systems, http://www.ingenuity.com). An IPA core analysis was performed focusing on both up- and down-regulated molecules and setting the log ratio (LR) cutoff ≥ 0.58 (fold change ≥ 1.5) and the FDR cutoff ≤ 0.0005 (range 0.0 to 0.0005).

SUPPLEMENTAL INFORMATION

Supplemental Information includes Supplemental Experimental Procedures, seven figures, and one table.

AUTHOR CONTRIBUTIONS

S.M.S, D.S, S.L., J.T., designed research;
S.M.S, K.H, A.M., L.F.R. and N.V. performed research;
S.L, J.T, D.D, B.D.S, and J.D.W contributed reagents/analytical tools;
S.M.S, S.L, W.V.D, and S.P. analyzed data;
and S.M.S and D.S wrote the paper.

ACKNOWLEDGEMENTS

For RNA-sequencing library preparation, sequencing and statistical analysis were performed by VIB Nucleomics Core (www.nucleomics.be). Siegfried Nebel helped with Fiji macros.
This work was supported by the Fonds voor Wetenschappelijk Onderzoek (FWO), the KU Leuven and VIB, a Methusalem grant from the KU Leuven/Flemish Government to BDS. BDS is supported by the Bax-Vanluffelen Chair for Alzheimer's Disease and "Opening the Future" of the Leuven Universiteit Fonds (LUF). BDS is supported by Vlaams Initiatief voor Netwerken voor Dementie Onderzoek (VIND, Strategic Basic Research Grant 135043).

REFERNCES

Agarwala, K.L., Ganesh, S., Tsutsumi, Y., Suzuki, T., Amano, K., and Yamakawa, K. (2001). Cloning and functional characterization of DSCAML1, a novel DSCAM-like cell adhesion molecule that mediates homophilic intercellular adhesion. Biochem Biophys Res Commun *285*, 760-772.

Alves-Sampaio, A., Troca-Marin, J.A., and Montesinos, M.L. (2010). NMDA-mediated regulation of DSCAM dendritic local translation is lost in a mouse model of Down's syndrome. The Journal of neuroscience : the official journal of the Society for Neuroscience *30*, 13537-13548.

Amano, K., Sago, H., Uchikawa, C., Suzuki, T., Kotliarova, S.E., Nukina, N., Epstein, C.J., and Yamakawa, K. (2004). Dosage-dependent over-expression of genes in the trisomic region of Ts1Cje mouse model for Down syndrome. Hum Mol Genet *13*, 1333-1340.

Aranda, S., Alvarez, M., Turro, S., Laguna, A., and de la Luna, S. (2008). Sprouty2-mediated inhibition of fibroblast growth factor signaling is modulated by the protein kinase DYRK1A. Molecular and cellular biology *28*, 5899-5911.

Bahn, S., Mimmack, M., Ryan, M., Caldwell, M.A., Jauniaux, E., Starkey, M., Svendsen, C.N., and Emson, P. (2002). Neuronal target genes of the neuron-restrictive silencer factor in neurospheres derived from fetuses with Down's syndrome: a gene expression study. Lancet *359*, 310-315.

Bao, J., Lin, H., Ouyang, Y., Lei, D., Osman, A., Kim, T.W., Mei, L., Dai, P., Ohlemiller, K.K., and Ambron, R.T. (2004). Activity-dependent transcription regulation of PSD-95 by neuregulin-1 and Eos. Nat Neurosci *7*, 1250-1258.

Barlow, G.M., Lyons, G.E., Richardson, J.A., Sarnat, H.B., and Korenberg, J.R. (2002). DSCAM: an endogenous promoter drives expression in the developing CNS and neural crest. Biochem Biophys Res Commun *299*, 1-6.

Becker, W., Weber, Y., Wetzel, K., Eirmbter, K., Tejedor, F.J., and Joost, H.G. (1998). Sequence characteristics, subcellular localization, and substrate specificity of DYRK-related kinases, a novel family of dual specificity protein kinases. J Biol Chem *273*, 25893-25902.

Bray, S.J. (2006). Notch signalling: a simple pathway becomes complex. Nat Rev Mol Cell Biol *7*, 678-689.

Cao, X., and Sudhof, T.C. (2001). A transcriptionally [correction of transcriptively] active complex of APP with Fe65 and histone acetyltransferase Tip60. Science *293*, 115-120.

Chao, H.W., Lai, Y.T., Lu, Y.L., Lin, C.L., Mai, W., and Huang, Y.S. (2012a). NMDAR signaling facilitates the IPO5-mediated nuclear import of CPEB3. Nucleic acids research *40*, 8484-8498.

Chao, H.W., Lai, Y.T., Lu, Y.L., Lin, C.L., Mai, W., and Huang, Y.S. (2012b). NMDAR signaling facilitates the IPO5-mediated nuclear import of CPEB3. Nucleic Acids Res *40*, 8484-8498.

Chen, B.E., Kondo, M., Garnier, A., Watson, F.L., Puettmann-Holgado, R., Lamar, D.R., and Schmucker, D. (2006). The molecular diversity of Dscam is functionally required for neuronal wiring specificity in Drosophila. Cell *125*, 607-620.

Cui, S., Lao, L., Duan, J., Jin, G., and Hou, X. (2013). Tyrosine phosphorylation is essential for DSCAML1 to promote dendrite arborization of mouse cortical neurons. Neurosci Lett *555*, 193-197.

Cvetkovska, V., Hibbert, A.D., Emran, F., and Chen, B.E. (2013). Overexpression of Down syndrome cell adhesion molecule impairs precise synaptic targeting. Nat Neurosci *16*, 677-682.

Dascenco, D., Erfurth, M.L., Izadifar, A., Song, M., Sachse, S., Bortnick, R., Urwyler, O., Petrovic, M., Ayaz, D., He, H.*, et al.* (2015). Slit and Receptor Tyrosine Phosphatase 69D Confer Spatial Specificity to Axon Branching via Dscam1. Cell *162*, 1140-1154.

David, M., Wong, L., Flavell, R., Thompson, S.A., Wells, A., Larner, A.C., and Johnson, G.R. (1996). STAT activation by epidermal growth factor (EGF) and amphiregulin. Requirement for the EGF receptor kinase but not for tyrosine phosphorylation sites or JAK1. J Biol Chem *271*, 9185-9188.

Di Vona, C., Bezdan, D., Islam, A.B., Salichs, E., Lopez-Bigas, N., Ossowski, S., and de la Luna, S. (2015). Chromatin-wide profiling of DYRK1A reveals a role as a gene-specific RNA polymerase II CTD kinase. Mol Cell *57*, 506-520.

Eyckerman, S., Verhee, A., der Heyden, J.V., Lemmens, I., Ostade, X.V., Vandekerckhove, J., and Tavernier, J. (2001). Design and application of a cytokine-receptor-based interaction trap. Nature cell biology *3*, 1114-1119.

Freitas, N., and Cunha, C. (2009). Mechanisms and signals for the nuclear import of proteins. Current genomics *10*, 550-557.

Fuerst, P.G., Bruce, F., Tian, M., Wei, W., Elstrott, J., Feller, M.B., Erskine, L., Singer, J.H., and Burgess, R.W. (2009). DSCAM and DSCAML1 function in self-avoidance in multiple cell types in the developing mouse retina. Neuron *64*, 484-497.
Fuerst, P.G., Harris, B.S., Johnson, K.R., and Burgess, R.W. (2010). A novel null allele of mouse DSCAM survives to adulthood on an inbred C3H background with reduced phenotypic variability. Genesis *48*, 578-584.
Fuerst, P.G., Koizumi, A., Masland, R.H., and Burgess, R.W. (2008). Neurite arborization and mosaic spacing in the mouse retina require DSCAM. Nature *451*, 470-474.
Goldschneider, D., Rama, N., Guix, C., and Mehlen, P. (2008). The neogenin intracellular domain regulates gene transcription via nuclear translocation. Mol Cell Biol *28*, 4068-4079.
Guedj, F., Pennings, J.L., Ferres, M.A., Graham, L.C., Wick, H.C., Miczek, K.A., Slonim, D.K., and Bianchi, D.W. (2015a). The fetal brain transcriptome and neonatal behavioral phenotype in the Ts1Cje mouse model of Down syndrome. Am J Med Genet A *167*, 1993-2008.
Guedj, F., Pennings, J.L., Wick, H.C., and Bianchi, D.W. (2015b). Analysis of adult cerebral cortex and hippocampus transcriptomes reveals unique molecular changes in the Ts1Cje mouse model of down syndrome. Brain pathology *25*, 11-23.
Hall, A. (1998). Rho GTPases and the actin cytoskeleton. Science *279*, 509-514.
Hanz, S., Perlson, E., Willis, D., Zheng, J.Q., Massarwa, R., Huerta, J.J., Koltzenburg, M., Kohler, M., van-Minnen, J., Twiss, J.L.*, et al.* (2003). Axoplasmic importins enable retrograde injury signaling in lesioned nerve. Neuron *40*, 1095-1104.
Hattori, D., Millard, S.S., Wojtowicz, W.M., and Zipursky, S.L. (2008). Dscam-mediated cell recognition regulates neural circuit formation. Annu Rev Cell Dev Biol *24*, 597-620.
He, H., Kise, Y., Izadifar, A., Urwyler, O., Ayaz, D., Parthasarthy, A., Yan, B., Erfurth, M.L., Dascenco, D., and Schmucker, D. (2014). Cell-intrinsic requirement of Dscam1 isoform diversity for axon collateral formation. Science *344*, 1182-1186.
Hing, H., Xiao, J., Harden, N., Lim, L., and Zipursky, S.L. (1999). Pak functions downstream of Dock to regulate photoreceptor axon guidance in Drosophila. Cell *97*, 853-863.
Huang, H., Shao, Q., Qu, C., Yang, T., Dwyer, T., and Liu, G. (2015). Coordinated interaction of Down syndrome cell adhesion molecule and deleted in colorectal cancer with dynamic TUBB3 mediates Netrin-1-induced axon branching. Neuroscience *293*, 109-122.
Hughes, M.E., Bortnick, R., Tsubouchi, A., Baumer, P., Kondo, M., Uemura, T., and Schmucker, D. (2007). Homophilic Dscam interactions control complex dendrite morphogenesis. Neuron *54*, 417-427.
Hummel, T., Vasconcelos, M.L., Clemens, J.C., Fishilevich, Y., Vosshall, L.B., and Zipursky, S.L. (2003). Axonal targeting of olfactory receptor neurons in Drosophila is controlled by Dscam. Neuron *37*, 221-231.
Jain, S., and Welshhans, K. (2016). Netrin-1 induces local translation of down syndrome cell adhesion molecule in axonal growth cones. Developmental neurobiology *76*, 799-816.
Jeffrey, R.A., Ch'ng, T.H., O'Dell, T.J., and Martin, K.C. (2009). Activity-dependent anchoring of importin alpha at the synapse involves regulated binding to the cytoplasmic tail of the NR1-1a subunit of the NMDA receptor. J Neurosci *29*, 15613-15620.
Jia, Y.L., Jing, L.J., Li, J.Y., Lu, J.J., Han, R., Wang, S.Y., Peng, T., and Jia, Y.J. (2011). Expression and significance of DSCAM in the cerebral cortex of APP transgenic mice. Neurosci Lett *491*, 153-157.
Kaech, S., and Banker, G. (2006). Culturing hippocampal neurons. Nat Protoc *1*, 2406-2415.
Karlstrom, H., Bergman, A., Lendahl, U., Naslund, J., and Lundkvist, J. (2002). A sensitive and quantitative assay for measuring cleavage of presenilin substrates. J Biol Chem *277*, 6763-6766.
Kim, J.H., Wang, X., Coolon, R., and Ye, B. (2013). Dscam expression levels determine presynaptic arbor sizes in Drosophila sensory neurons. Neuron *78*, 827-838.
Kise, Y., and Schmucker, D. (2013). Role of self-avoidance in neuronal wiring. Curr Opin Neurobiol *23*, 983-989.
Ko, J., Fuccillo, M.V., Malenka, R.C., and Sudhof, T.C. (2009). LRRTM2 functions as a neurexin ligand in promoting excitatory synapse formation. Neuron *64*, 791-798.
Kopan, R., Schroeter, E.H., Weintraub, H., and Nye, J.S. (1996). Signal transduction by activated mNotch: importance of proteolytic processing and its regulation by the extracellular domain. Proc Natl Acad Sci U S A *93*, 1683-1688.
Leder, S., Weber, Y., Altafaj, X., Estivill, X., Joost, H.G., and Becker, W. (1999). Cloning and characterization of DYRK1B, a novel member of the DYRK family of protein kinases. Biochem Biophys Res Commun *254*, 474-479.

Lever, M.B., Karpova, A., and Kreutz, M.R. (2015). An Importin Code in neuronal transport from synapse-to-nucleus? Frontiers in molecular neuroscience *8*, 33.
Li, H.L., Huang, B.S., Vishwasrao, H., Sutedja, N., Chen, W., Jin, I., Hawkins, R.D., Bailey, C.H., and Kandel, E.R. (2009). Dscam mediates remodeling of glutamate receptors in Aplysia during de novo and learning-related synapse formation. Neuron *61*, 527-540.
Li, S., Sukeena, J.M., Simmons, A.B., Hansen, E.J., Nuhn, R.E., Samuels, I.S., and Fuerst, P.G. (2015). DSCAM promotes refinement in the mouse retina through cell death and restriction of exploring dendrites. J Neurosci *35*, 5640-5654.
Lievens, S., Peelman, F., De Bosscher, K., Lemmens, I., and Tavernier, J. (2011). MAPPIT: a protein interaction toolbox built on insights in cytokine receptor signaling. Cytokine Growth Factor Rev *22*, 321-329.
Lievens, S., Vanderroost, N., Van der Heyden, J., Gesellchen, V., Vidal, M., and Tavernier, J. (2009). Array MAPPIT: high-throughput interactome analysis in mammalian cells. J Proteome Res *8*, 877-886.
Lim, S., Jin, K., and Friedman, E. (2002). Mirk protein kinase is activated by MKK3 and functions as a transcriptional activator of HNF1alpha. J Biol Chem *277*, 25040-25046.
Liu, F., Liang, Z., Wegiel, J., Hwang, Y.W., Iqbal, K., Grundke-Iqbal, I., Ramakrishna, N., and Gong, C.X. (2008). Overexpression of Dyrk1A contributes to neurofibrillary degeneration in Down syndrome. FASEB J *22*, 3224-3233.
Liu, G., Li, W., Wang, L., Kar, A., Guan, K.L., Rao, Y., and Wu, J.Y. (2009). DSCAM functions as a netrin receptor in commissural axon pathfinding. Proceedings of the National Academy of Sciences of the United States of America *106*, 2951-2956.
Lowe, S.A., Hodge, J.J.L., and Usowicz, M.M. (2018). A third copy of the Down syndrome cell adhesion molecule (Dscam) causes synaptic and locomotor dysfunction in Drosophila. Neurobiol Dis *110*, 93-101.
Lu, B., Pang, P.T., and Woo, N.H. (2005). The yin and yang of neurotrophin action. Nat Rev Neurosci *6*, 603-614.
Ly, A., Nikolaev, A., Suresh, G., Zheng, Y., Tessier-Lavigne, M., and Stein, E. (2008). DSCAM is a netrin receptor that collaborates with DCC in mediating turning responses to netrin-1. Cell *133*, 1241-1254.
Manser, E., Leung, T., Salihuddin, H., Zhao, Z.S., and Lim, L. (1994). A brain serine/threonine protein kinase activated by Cdc42 and Rac1. Nature *367*, 40-46.
Marti, F., Garcia, G.G., Lapinski, P.E., MacGregor, J.N., and King, P.D. (2006). Essential role of the T cell-specific adapter protein in the activation of LCK in peripheral T cells. J Exp Med *203*, 281-287.
Matthews, B.J., Kim, M.E., Flanagan, J.J., Hattori, D., Clemens, J.C., Zipursky, S.L., and Grueber, W.B. (2007). Dendrite self-avoidance is controlled by Dscam. Cell *129*, 593-604.
May, P., Reddy, Y.K., and Herz, J. (2002). Proteolytic processing of low density lipoprotein receptor-related protein mediates regulated release of its intracellular domain. J Biol Chem *277*, 18736-18743.
Millard, S.S., Lu, Z., Zipursky, S.L., and Meinertzhagen, I.A. (2010). Drosophila dscam proteins regulate postsynaptic specificity at multiple-contact synapses. Neuron *67*, 761-768.
Miyamoto, Y., Yamada, K., and Yoneda, Y. (2016). Importin alpha: a key molecule in nuclear transport and non-transport functions. J Biochem *160*, 69-75.
Mosca, T.J., and Schwarz, T.L. (2010). The nuclear import of Frizzled2-C by Importins-beta11 and alpha2 promotes postsynaptic development. Nat Neurosci *13*, 935-943.
Nakagawa, T., Kajitani, T., Togo, S., Masuko, N., Ohdan, H., Hishikawa, Y., Koji, T., Matsuyama, T., Ikura, T., Muramatsu, M*., et al.* (2008). Deubiquitylation of histone H2A activates transcriptional initiation via trans-histone cross-talk with H3K4 di- and trimethylation. Genes Dev *22*, 37-49.
Neuhaus-Follini, A., and Bashaw, G.J. (2015). The Intracellular Domain of the Frazzled/DCC Receptor Is a Transcription Factor Required for Commissural Axon Guidance. Neuron *87*, 751-763.
Okumura, M., Sakuma, C., Miura, M., and Chihara, T. (2015). Linking cell surface receptors to microtubules: tubulin folding cofactor D mediates Dscam functions during neuronal morphogenesis. J Neurosci *35*, 1979-1990.
Panayotis, N., Karpova, A., Kreutz, M.R., and Fainzilber, M. (2015). Macromolecular transport in synapse to nucleus communication. Trends Neurosci *38*, 108-116.
Park, H., and Poo, M.M. (2013). Neurotrophin regulation of neural circuit development and function. Nat Rev Neurosci *14*, 7-23.

Perry, R.B., Doron-Mandel, E., Iavnilovitch, E., Rishal, I., Dagan, S.Y., Tsoory, M., Coppola, G., McDonald, M.K., Gomes, C., Geschwind, D.H., *et al.* (2012). Subcellular knockout of importin beta1 perturbs axonal retrograde signaling. Neuron *75*, 294-305.
Purohit, A.A., Li, W., Qu, C., Dwyer, T., Shao, Q., Guan, K.L., and Liu, G. (2012). Down syndrome cell adhesion molecule (DSCAM) associates with uncoordinated-5C (UNC5C) in netrin-1-mediated growth cone collapse. The Journal of biological chemistry *287*, 27126-27138.
Reich, N.C., and Liu, L. (2006). Tracking STAT nuclear traffic. Nature reviews Immunology *6*, 602-612.
Saito, Y., Oka, A., Mizuguchi, M., Motonaga, K., Mori, Y., Becker, L.E., Arima, K., Miyauchi, J., and Takashima, S. (2000). The developmental and aging changes of Down's syndrome cell adhesion molecule expression in normal and Down's syndrome brains. Acta Neuropathol *100*, 654-664.
Savas, J.N., Ribeiro, L.F., Wierda, K.D., Wright, R., DeNardo-Wilke, L.A., Rice, H.C., Chamma, I., Wang, Y.Z., Zemla, R., Lavallee-Adam, M., *et al.* (2015). The Sorting Receptor SorCS1 Regulates Trafficking of Neurexin and AMPA Receptors. Neuron *87*, 764-780.
Schindelin, J., Arganda-Carreras, I., Frise, E., Kaynig, V., Longair, M., Pietzsch, T., Preibisch, S., Rueden, C., Saalfeld, S., Schmid, B., *et al.* (2012). Fiji: an open-source platform for biological-image analysis. Nature methods *9*, 676-682.
Schmucker, D., Clemens, J.C., Shu, H., Worby, C.A., Xiao, J., Muda, M., Dixon, J.E., and Zipursky, S.L. (2000). Drosophila Dscam is an axon guidance receptor exhibiting extraordinary molecular diversity. Cell *101*, 671-684.
Schramm, R.D., Li, S., Harris, B.S., Rounds, R.P., Burgess, R.W., Ytreberg, F.M., and Fuerst, P.G. (2012). A novel mouse Dscam mutation inhibits localization and shedding of DSCAM. PloS one *7*, e52652.
Shindoh, N., Kudoh, J., Maeda, H., Yamaki, A., Minoshima, S., Shimizu, Y., and Shimizu, N. (1996). Cloning of a human homolog of the Drosophila minibrain/rat Dyrk gene from "the Down syndrome critical region" of chromosome 21. Biochem Biophys Res Commun *225*, 92-99.
Simicek, M., Lievens, S., Laga, M., Guzenko, D., Aushev, V.N., Kalev, P., Baietti, M.F., Strelkov, S.V., Gevaert, K., Tavernier, J., *et al.* (2013). The deubiquitylase USP33 discriminates between RALB functions in autophagy and innate immune response. Nature cell biology *15*, 1220-1230.
Simmons, A.B., Bloomsburg, S.J., Sukeena, J.M., Miller, C.J., Ortega-Burgos, Y., Borghuis, B.G., and Fuerst, P.G. (2017). DSCAM-mediated control of dendritic and axonal arbor outgrowth enforces tiling and inhibits synaptic plasticity. Proc Natl Acad Sci U S A *114*, E10224-E10233.
Soba, P., Zhu, S., Emoto, K., Younger, S., Yang, S.J., Yu, H.H., Lee, T., Jan, L.Y., and Jan, Y.N. (2007). Drosophila sensory neurons require Dscam for dendritic self-avoidance and proper dendritic field organization. Neuron *54*, 403-416.
Soundararajan, M., Roos, A.K., Savitsky, P., Filippakopoulos, P., Kettenbach, A.N., Olsen, J.V., Gerber, S.A., Eswaran, J., Knapp, S., and Elkins, J.M. (2013). Structures of Down syndrome kinases, DYRKs, reveal mechanisms of kinase activation and substrate recognition. Structure *21*, 986-996.
Steiner, H., and Haass, C. (2000). Intramembrane proteolysis by presenilins. Nat Rev Mol Cell Biol *1*, 217-224.
Sterne, G.R., Kim, J.H., and Ye, B. (2015). Dysregulated Dscam levels act through Abelson tyrosine kinase to enlarge presynaptic arbors. eLife *4*.
Struhl, G., and Adachi, A. (2000). Requirements for presenilin-dependent cleavage of notch and other transmembrane proteins. Mol Cell *6*, 625-636.
Sun, W., You, X., Gogol-Doring, A., He, H., Kise, Y., Sohn, M., Chen, T., Klebes, A., Schmucker, D., and Chen, W. (2013). Ultra-deep profiling of alternatively spliced Drosophila Dscam isoforms by circularization-assisted multi-segment sequencing. The EMBO journal *32*, 2029-2038.
Taniguchi, Y., Kim, S.H., and Sisodia, S.S. (2003). Presenilin-dependent "gamma-secretase" processing of deleted in colorectal cancer (DCC). J Biol Chem *278*, 30425-30428.
Thompson, K.R., Otis, K.O., Chen, D.Y., Zhao, Y., O'Dell, T.J., and Martin, K.C. (2004). Synapse to nucleus signaling during long-term synaptic plasticity; a role for the classical active nuclear import pathway. Neuron *44*, 997-1009.
Tinti, M., Kiemer, L., Costa, S., Miller, M.L., Sacco, F., Olsen, J.V., Carducci, M., Paoluzi, S., Langone, F., Workman, C.T., *et al.* (2013). The SH2 domain interaction landscape. Cell Rep *3*, 1293-1305.
Watson, F.L., Puttmann-Holgado, R., Thomas, F., Lamar, D.L., Hughes, M., Kondo, M., Rebel, V.I., and Schmucker, D. (2005). Extensive diversity of Ig-superfamily proteins in the immune system of insects. Science *309*, 1874-1878.

Xu, D., Farmer, A., and Chook, Y.M. (2010). Recognition of nuclear targeting signals by Karyopherin-beta proteins. Curr Opin Struct Biol *20*, 782-790.
Yamagata, M., and Sanes, J.R. (2008). Dscam and Sidekick proteins direct lamina-specific synaptic connections in vertebrate retina. Nature *451*, 465-469.
Yamagata, M., and Sanes, J.R. (2010a). Synaptic localization and function of Sidekick recognition molecules require MAGI scaffolding proteins. J Neurosci *30*, 3579-3588.
Yamagata, M., and Sanes, J.R. (2010b). Synaptic localization and function of Sidekick recognition molecules require MAGI scaffolding proteins. The Journal of neuroscience : the official journal of the Society for Neuroscience *30*, 3579-3588.
Yamakawa, K., Huot, Y.K., Haendelt, M.A., Hubert, R., Chen, X.N., Lyons, G.E., and Korenberg, J.R. (1998). DSCAM: a novel member of the immunoglobulin superfamily maps in a Down syndrome region and is involved in the development of the nervous system. Hum Mol Genet *7*, 227-237.
Yang, L., Garbe, D.S., and Bashaw, G.J. (2009). A frazzled/DCC-dependent transcriptional switch regulates midline axon guidance. Science *324*, 944-947.
Yaseen, N.R., and Blobel, G. (1997). Cloning and characterization of human karyopherin beta3. Proc Natl Acad Sci U S A *94*, 4451-4456.

Figure Legends Main Figures

Figure 1
DSCAMs interact with DYRK1A, DYRK1B and IPO5.
(A) Schematic of the MAPPIT technique. The mouse DSCAM or DSCAML1 ICDs were fused to the C-terminus of a signaling deficient leptin receptor (LR) fragment lacking STAT3 recruitment sites (tyrosines) and used as baits. The preys are tethered to a gp130 cytokine receptor fragment containing functional STAT3 sites. Upon leptin stimulation, association of bait and prey restores a functional leptin receptor complex resulting in STAT3 activation, which can be monitored by a STAT3-responsive luciferase reporter. P, phospho-tyrosine. JAK, janus kinase.
(B) DSCAM interacts with DYRK1A and -B. LR-DSCAM and LR-eDHFR (negative control bait) baits were introduced in HEK cells together with a DYRK1A prey, DYRK1B prey, empty prey (negative control) or an EFHA1 prey (positive control) and binding was tested in MAPPIT. Results for DSCAML1 are shown in Figure S1B.
(C) Schematic of full-length (FL) DYRK1A, DYRK1B and truncated DYRK1A/B preys. DYRK1A contains a nuclear localization signal, a protein kinase domain, a leucine zipper motif, and a highly conserved ploy-histidine repeat; DYRK1B lacks the poly-histidine repeat.
(D-E) The interactions between truncated DYRK1A (aa 1-482) or DYRK1B (aa 558-629) preys and the DSCAM (LR-DSCAM^{Y1746F}) bait (i.e. suppressing STAT3-mediated background) were assayed using MAPPIT. Results for DSCAML1 are shown in Figure S3 A-B.
(D) The C-terminus of DYRK1B is sufficient for the interaction with DSCAM and the kinase domain is not required.
(E) The DYRK1A kinase domain is not sufficient to bind to DSCAM.
(F) Mutation of the potential DYRK kinase substrate site does not inhibit the interaction between DSCAM and DYRK1A or DYRK1B. A potential substrate site for DYRKs was mutated in the DSCAM bait (RPGT to AAGA). The interactions of mutant or wild type DSCAM baits with DYRK1A, DYRK1B as well as IPO5 (positive control prey) were tested in a binary MAPPIT experiments. Results for DSCAML1 are shown in Figure S3 C-D.
(G) DSCAM and DSCAML1 strongly interact with IPO5. LR-DSCAM, LR-DSCAML1, and LR-eDHFR (negative control bait) baits were introduced in HEK cells together with an IPO5 prey, an empty prey (negative control) or an EFHA1 prey (positive control) and binding was tested in MAPPIT.
(H) DSCAMs exhibit a conserved NLS. Green, monopartite NLS motif predicted by NLS Mapper.
(I) Loss of the NLSs of DSCAMs inhibits binding of IPO5. Binding of IPO5 to wt or mutant DSCAM and DSCAML1 baits lacking the NLS (LR-DSCAM$^{\Delta NLS}$, LR-DSCAML1$^{\Delta NLS}$) was tested in MAPPIT. Negative control, empty prey. Positive control, STAT3 prey.
(J) The interaction between DSCAMs and IPO5 is specific. The interaction between 9 importin preys and the DSCAM^{Y1746F} or the DSCAML1$^{Y1744/1937F}$ bait (i.e. suppressing STAT3-mediated background signal) was evaluated in a binary MAPPIT experiment and the expression of the importin preys was confirmed by Western Blot.
(B-G) and (I-J) Bar graphs show the mean ± SD of fold induction from samples assayed in triplicates. Fold induction is the ratio between the average luciferase activities of the ligand-treated and the ligand-untreated samples. Results shown are representative for three independent experiments. Negative control, empty prey only consisting of the gp130 fragment.

Table 1. Binding partners of DSCAMs identified with MAPPIT. Further validation of the candidates can be found in Figure S1, S2, and S3.

Figure 2. DSCAM family Ig-CAMs are cleaved releasing their ICDs.
(A) Schematic of C-terminally HA-tagged DSCAM and DSCAML1 constructs. ECD, extracellular domain. TM, transmembrane domain. ICD, intracellular domain. HA, human influenza hemagglutinin epitope.
(B) Immunoblot showing C-terminal ICD fragments resulting from cleavage of DSCAM and DSCAML1. Constructs shown in A were expressed in HEK293 cells, immunoprecipitated and subsequently immunoblotted using an HA-antibody. Control, HA-tagged YFP.
(C) Schematic of the cleavage reporter assay. DSCAM or DSCAML1 were fused to the DNA-binding domain of Gal4 (Gal4DBD) and the transcriptional activation domain of VP16 (VP16TAD). Intra-membrane cleavage results in nuclear translocation of cleaved fragments and activation of a Luciferase reporter in the nucleus.
(D) Cleavage reporter assay confirming cleavage of DSCAMs. HEK293 cells were transfected with DSCAM-, DSCAML1-, IFNaR1-, or IFNaR2-Gal4DBD-VP16 or Gal4DBD-VP16 alone and co-transfected with Gal50hIL6luc and pRL-TK and luciferase activity was quantified after 24h. Results are expressed as relative luciferase units (RLU), which are calculated as the ratio of firefly (Gal50hIL6luc) and renilla (pRL-TK) luciferase activities. All values were normalized to the RLU of IFNaR1-Gal4DBD-VP16. Bar graphs show the mean ± SD of samples assayed in triplicate. A representative experiment out of 3 independent experiments is shown.
(E) Immunoblot showing *Drosophila* Dscam 1 cleavage *in vivo*. Brain lysates from wt and from transgenic Dscam1-HA-Flag tagged flies (i.e. endogenous tag within the ICD of the *Dscam1* gene) were immuno-blotted and probed with HA-specific and Dscam1-ICD-specific antibodies.
(F) DSCAM is cleaved by γ-secretase. HA-immunoblot from lysates of DSCAM-HA expressing stable HEK293 cells treated over night with DMSO, or Lactacystin (10 μM) in the presence or absence of the gamma-secretase inhibitors DAPT (10 μM) or inhibitor X (10 μM).
(G) Model of secretase-mediated DSCAM cleavage according to our results and literature on related secretase-cleaved receptors.

Figure 3. The NLSs of DSCAMs are required for nuclear translocation of their ICDs.
(A) Schematic of YFP-tagged DSCAM and DSCAML1 constructs used in D-I. A C-terminal YFP-HA tag was fused to the ICDs of DSCAMs, to ICD constructs lacking the NLS ($ICD^{\Delta NLS}$), and to full-length DSCAM/L1.
(B-D) YFP-tagged DSCAM/L1 constructs shown in (A) were expressed in HEK293 cells and cells were stained with DAPI to visualize the nuclei and imaged for YFP (yellow) and DAPI (cyan) fluorescence.
(B) The ICDs of DSCAM and DSCAML1 localize to the nucleus of HEK293 cells.
(C) Deletion of the NLSs impairs nuclear localization of the DSCAM and DSCAML1 ICDs. Subcellular localization of DSCAM/L1 $ICD^{\Delta NLS}$ constructs in HEK293 cells.
(D) Subcellular localization of YFP-HA tagged full-length DSCAM and DSCAML1 in HEK293 cells.
(E-G) YFP-tagged DSCAM/L1 constructs shown in (A) were expressed in primary mouse cortical neurons at E14.5 and cells were immuno-stained with DAPI (cyan) and an anti-YFP/GFP antibody (yellow).
(E) The ICDs of DSCAMs enrich in the nucleus of primary neurons.
(F) DSCAM/L1 $ICD^{\Delta NLS}$ constructs (i.e. lacking the NLS) are localized in the cytoplasm of primary cortical neurons.
(G) Subcellular localization of full-length DSCAM and DSCAML1 in primary cortical neurons.
(B-G) Scale bars, 10 μM. Single confocal planes are shown.

Figure 4. The ICDs of DSCAM and DSCAML1 modulate the Expression of Genes Involved in Neuronal Circuit Formation.
(A) Outline of RNA-Sequencing experiment.

(B – E) Results of Ingenuity Pathway Core Analysis (FDR ≤ 0.0005; LR ≥ 0.58, ≤ -0.58) comparing the transcriptomes of stable cell lines expressing the DSCAM–ICD vs. YFP-NLS, or DSCAML1-ICD vs. YFP-NLS. Genes that changed expression in nuclear vs. cytoplasmic YFP controls (YFP-NLS vs. YFP-CYT) were stringently excluded from the analysis (FDR ≤ 0.1). DEGs, differentially expressed genes.
(B) Bar graph showing the number of up- and down-regulated genes in the DSCAM and DSCAML1 data sets.
(C) Venn diagram showing the number of overlapping and individual DEGs between the DSCAM and DSCAML1 data sets.
(D) Selection of DEGs involved in neuronal circuit formation and function in DSCAM-ICD relative to YFP-NLS-expressing cells.
(E) Selection of DEGs involved in neuronal circuit formation and function in DSCAML1-ICD relative to YFP-NLS-expressing cells.
(D-E). Up- and down regulation is expressed as log ratio (i.e. log2 fold change). Positive log ratio, up-regulation (green). Negative log ratio, down- regulation (magenta).

Figure 5. Nuclear translocation of the ICDs of DSCAMs impairs neurite outgrowth in primary cortical neurons.
(A) Schematic of C-terminally YFP-HA tagged lentiviral DSCAM and DSCAML1 constructs expressed in B.
(B) Neuron specific tubulin (Tuj1) staining showing the morphology of primary cortical neurons transduced with lentiviral expression constructs shown in A. Primary cortical cultures from E14.5 mouse embryos were transduced with lentivirus at DIV1 and immune-stained at DIV4 with anti-Tuj1, anti-GFP/YFP, and DAPI (to visualize cell bodies). Single confocal projections of YFP positive neurons are shown.
(C-D) Quantification of total neurite length and of the length of the longest neurite. The neuronal tubulin cytoskeleton was traced and the neurite length was determined using the ImageJ/Fiji software (see Methods). Total neurite length was calculated as the sum of length of all neurites of a given neuron in µm. The longest neurite of each neuron was measured in µm using the simple neurite tracing tool of Fiji. Bar graphs show the mean ±SEM. P-values were calculated using the Prism7 software performing a Kruskal-Wallis test with Dunn's multiple comparisons test (****p ≤ 0.0001, ***p ≤ 0.001).
(C) Total neurite length and the length of the longest neurite are decreased in neurons expressing the DSCAM ICD as compared to control neurons expressing YFP or DSCAM-ICD$^{\Delta NLS}$.
(D) Total neurite length and the length of the longest neurite are decreased in neurons expressing the DSCAML1 ICD as compared to control neurons expressing YFP or DSCAML1-ICD$^{\Delta NLS}$.

Figure 6. The DSCAM but not the DSCAML1 ICD Affects Synapse Development of Hippocampal Neurons.
(A-D) Analysis of synapse density in E18 hippocampal neuron cultures electroporated with YFP-tagged DSCAM-ICD or full-length DSCAM (DSCAM-FL) in comparison to control neurons electroporated with YFP alone or YFP-tagged DSCAM-ICD$^{\Delta NLS}$.
(A, F, H and J) Electroporated hippocampal neurons were immuno-stained on DIV10 for YFP, PSD95, VGlut1, and MAP2 and YFP-positive neurons were imaged.
(A, F and J) Overview images of VGlut1-positive puncta. Scale bars, 20 µm. Magnifications show single dendrites (boxes) with synapses visualized by Vglut1 and PSD95 staining. Scale bars, 5 µm.
(B-D) Vglut1-, PSD95-, and double-positive puncta density is decreased in DSCAM-ICD and DSCAM-FL expressing neurons as compared to control neurons expressing YFP (****p ≤ 0.0001) or DSCAM-ICD$^{\Delta NLS}$ ($^{++++}$p ≤ 0.0001, $^{+++}$p ≤ 0.001).

(B) Vglut1-, and PSD95- double-positive puncta normalized to dendritic length (synapse density).
(C) Vglut1-positive puncta normalized to dendritic length.
(D) PSD95- positive puncta normalized to dendritic length.
(E-G) The DSCAM ICD has a cell non-autonomous effect. Reduced synapse density in cultures electroporated with the DSCAM-ICD in both, transfected (DSCAM ICD TF) and neighboring non-transfected neurons (DSCAM ICD NTF) as compared to control neurons expressing YFP (****$p \leq 0.0001$, $^{\#}p \leq 0.05$).
(H) Subcellular localization of recombinant YFP-tagged full-length DSCAM or DSCAML1 in hippocampal neurons. Scale bars, 10 µm.
(J-M) Synapse density in hippocampal neuron cultures electroporated with YFP-tagged DSCAML1-ICD or full-length DSCAML1 (DSCAML1-FL) in comparison to control neurons electroporated with YFP alone or YFP-tagged DSCAML1-ICD$^{\Delta NLS}$.
(K) Decreased synapse density in DSCAML1-FL expressing neurons as compared to control neurons expressing YFP (*$p \leq 0.05$).
(L) Decreased Vglut1-positive puncta density in DSCAML1-FL expressing neurons as compared to control neurons expressing YFP (*$p \leq 0.05$).
(M) Decreased PSD95-positive puncta density in DSCAML1-FL expressing neurons as compared to control neurons expressing YFP (***$p \leq 0.001$) or DSCAML1-ICD ($^{\#\#\#}p \leq 0.001$).
Bar graphs in (B), (C), (D), (G), (K), (L), and (M) show mean ±SEM and p-values by ordinary one-way Anova with Turkey's multiple comparisons test.

Figure 7. Model of Nuclear DSCAM Signaling.
γ-secretase mediated intra-membrane cleavage of DSCAM receptors results in the release of the DSCAM ICD, which is likely proceeded by shedding of the DSCAM ectodomain. Interaction of IPO5 with the NLS of DSCAM then leads to importin-mediated nuclear import of the DSCAM ICD. In the nucleus, the DSCAM ICD may regulate the transcription of genes involved in neuronal development and function, thereby regulating processes such as neurite outgrowth, branching, and repulsion, as well as synapse formation, axon guidance, and neuronal cell death.

Figure Legends Supplementary Figures

Figure S1 (related to Figure 1). Validation of the MAPPIT screening results.
(A-B) Binary MAPPIT experiments including control baits and preys to further validate the screening results of candidates not shown in main figures.
(A-D) LR-DSCAML1, LR-DSCAML1, EpoR-DSCAM and LR-eDHFR or EpoR-eDHFR (negative control baits) were used as baits and introduced into 293T cells together with the indicated preys and tested in binary MAPPIT experiments. Bar graphs show the mean ± SD of fold induction from samples assayed in triplicates. Fold induction is the ratio between the average luciferase activities of the ligand-treated and the ligand-untreated samples. Results shown are representative for three independent experiments. Negative control, empty prey only consisting of the gp130 fragment. Positive control, EFHA1 prey.
(A) DSCAM binds to SH2D2A, STAT3, and USP21.
(B) DSCAML1 binds to SH2D2A, STAT3, USP21, DYRK1A, and DYRK1B.
(C) DSCAM baits induce MAPPIT signals with known binding partners MAGI1 and PAK1.
(D) DSCAML1 baits induce MAPPIT signals with known binding partner MAGI1.

Figure S2 (related to Figure 1). Identification of tyrosine motifs serving as binding sites for STAT3, USP21 and SH2D2A.

(A) The ICDs of mouse DSCAM/L1 and Drosophila Dscam1exhibit conserved YxxQ consensus motifs, which represent potential binding sites for the SH2 domain of STAT3. YxxQ motifs were identified using the ELM platform.
(B-G) and (I-J) LR-DSCAML1, LR-DSCAML1, EpoR-DSCAM and LR-eDHFR (negative control bait) were used as baits and introduced into 293T cells together with the indicated preys and tested in binary MAPPIT experiments. Bar graphs show the mean ± SD of fold induction from samples assayed in triplicates. Fold induction is the ratio between the average luciferase activities of the ligand-treated and the ligand-untreated samples. Results shown are representative for three independent experiments. Negative control, empty prey only consisting of the gp130 fragment. Positive control, EFHA1 prey.
(B-C) Mutation of the YXXQ motif abolishes the interaction between DSCAM and STAT3 (B) or USP21 (C), whereas binding to IPO5 is not affected. Tyrosine residue 1746 was substituted for phenylalanine in the LR-DSCAM bait. An IPO5 prey was used as positive control.
(D), (G) Both LR-DSCAM and LR-DSCAML1 bait receptors gave rise to background in MAPPIT, i.e. generated a signal in the absence of an interaction as in the case when these baits are combined with an empty control prey consisting of only the gp130 receptor fragment. The background is strongly reduced with the STAT3 binding deficient LR-DSCAM^{Y1746F} and LR-DSCAML1$^{Y1744/1937F}$ bait receptors.
(E-F) Mutation of a single YXXQ motif reduces, and double mutation abolishes the interaction between DSCAML1 and STAT3 (E) or USP21 (F), whereas binding to IPO5 is not affected. Tyrosine residues 1744 and 1937 were substituted with phenylalanine in the LR-DSCAML1 bait.
(H) A YCNL motif is located around tyrosine residue 1898 in the DSCAML1 ICD. This motif represents a potential binding site for the SH2 domain of SH2D2A.
(I) Mutation of the YCNL motif abolishes the interaction between DSCAML1 and SH2D2A, whereas binding to IPO5 is not affected. Tyrosine residue 1898 was substituted for phenylalanine in the LR-DSCAML1 bait (DSCAML1^{Y1898F}).
(J) SH2DA does not bind to any DSCAM tyrosine. All 9 tyrosine residues in the DSCAM ICD were substituted for phenylalanine in the EpoR-DSCAM MAPPIT bait and tested in MAPPIT.
(A), (H) Tyrosine residues represent sequence positions of within the mouse cytoplasmic domains of DSCAM and DSCAML1.

Figure S3 (related to Figure 1). DSCAML1 interacts with DYRK1A and DYRK1B.
(A-B) The interactions between STAT3-binding deficient DSCAML1 bait (LR-DSCAML1$^{Y1744/1937F}$) and the DYRK1B (aa 558-629) or DYRK1A (aa 1-482) prey were assayed using MAPPIT.
(A) The C-terminus of DYRK1B is sufficient for the interaction with DSCAML1 and the kinase domains is not required.
(B) The DYRK1A kinase domain is not sufficient to bind to DSCAML1.
(C-D) DSCAMs exhibit a potential substrate site for DYRKs, which was mutated in the DSCAML1 bait (RPGT to AAGA). The interaction between mutant or wild type DSCAML1 baits and DYRK1A or DYRK1B as well as IPO5 (positive control prey) were tested in a binary MAPPIT experiment. Mutation of the potential DYRK kinase substrate site does not inhibit the interaction between DSCAML1 and DYRK1A or DYRK1B.
(A-D) Negative control: empty prey only consisting of the gp130 fragment. Bar graphs show the mean ± SD of fold induction, which is the ratio between the average luciferase activities of the ligand-treated and the ligand-untreated samples.

Figure S4 (related to Figure 2). Un-cropped western blot membrane shown in Figure 2F.
Dashed rectangle indicates the cropped region in Figure 2F. Full-length DSCAM migrates around 250 kDa and cleaved ICD fragments at about 50 kDa.

Figure S5 (related to Figure 4). Enriched Biological Functions in DSCAM and DSCAML1 RNA-seq datasets.
(A-B) Volcano plots showing all profiled up- and down- regulated genes as log2 fold change versus –log10 of the false discovery rate (FDR) corrected p-value in the DSCAM (A) and DSCAML1 (B) data sets. Statistically relevant DEGs are separated from statistically non-relevant DEGs by a horizontal striped line by FDR ≤ 0.0005 cut off. Vertical striped lines indicate the log ratio (LR) cut off (LR ≥ 0.58, ≤ -0.58; fold change ≥ 1.5, ≤ 1.5). For simplicity genes differentially expressed in nuclear vs. cytoplasmic YFP control cell lines (FDR ≥ 0.1) are not shown.
(A) Volcano plot showing all profiled genes in DSCAM ICD vs. nuclear YFP expressing cell lines. Note that DSCAM is highly up-regulated (log2 fold change, 6.0345; -log10 of p-value, 124.678) due to experimental overexpression of the DSCAM ICD.
(B) Volcano plot showing all profiled genes in DSCAML1 ICD vs. nuclear YFP expressing cell lines. DSCAML1 is highly up-regulated (log2 fold change, 7.553) due to experimental overexpression of the DSCAML1 ICD. The arrow indicates that due to a FDR p-value of 0, this data point cannot be plotted on a –log10 scale.
(C-D) Results of Ingenuity Pathway Core Analysis (FDR ≤ 0.0005; LR ≥ 0.58, ≤ -0.58). Enriched biological functions related to physiological system development and function and canonical pathways. X-axis shows likelihood of association between a set of genes in our dataset and a biological function, expressed as -log (p-value). Enriched biological functions and pathways were scored according to their p-value, calculated with the Fischer's exact test. The y-axis shows the annotations of the enriched biological functions or canonical pathways of differentially expressed genes.
(C) Functional classification of DEGs in DSCAM-ICD relative to YFP-NLS-expressing cells (p-value ≤ 0.05).
(D) Functional classification of DEGs in DSCAML1-ICD relative to YFP-NLS-expressing cells (p-value ≤ 0.05).

Table S1 (related to Figure 4). DEGs of the DSCAM data set related to axon guidance signaling identified by Ingenuity Pathway Core Analysis (FDR ≤ 0.0005; LR ≥ 0.58, ≤ -0.58).

Table S2 (related to figure 4). DEGs of the DSCAML1 data set related to axon guidance signaling identified by Ingenuity Pathway Core Analysis (FDR ≤ 0.0005; LR ≥ 0.58, ≤ -0.58).

Figure S6 (related to Figure 5). Neurite tracing of cortical neurons expressing recombinant YFP-tagged DSCAM or DSCAML1 constructs.
(A) Neuronal morphology of additional examples related to Figure 5B. Scale bars, 50 µm.
(B) Outline of semi-automatic neurite tracing in Fiji used to quantify the total neurite length of primary cortical neurons in Figure 5C.
(C) Comparison of quantification results obtained with semi-automatic tracing vs. manual neurite tracing using simple neurite tracer plugin of Fiji. 12-17 neurons (as indicated) were traced using both methods. The semi-automated tracing method does not take smaller branches and filopodia into account but nevertheless yielded similar ratios between conditions compared to labor-intensive manual tracing using the simple neurite tracer plugin of Fiji. P-values were calculated using the Prism7 software performing an ordinary one-way ANOVA with Tukeys's multiple comparisons test (*p ≤ 0.05, **p ≤ 0.01, ***p ≤ 0.001, ****p ≤ 0.0001).

Figure S7 (related to Figure 6).
(A) Split color channels of MAP2, YFP, PSD95, and VGlut1 immuno-staining shown in Figure 6A.
(B) Split color channels of MAP2, YFP, PSD95, and VGlut1 immuno-staining shown in Figure 6F.

(C) Reduced Vglut1 density in cultures electroporated with the DSCAM-ICD in both, transfected (DSCAM ICD (+)) and neighboring non-transfected neurons (DSCAM ICD (-)) as compared to control neurons expressing YFP (****$p \leq 0.0001$, **$p \leq 0.01$). Vglut1 density is significantly reduced in transfected (DSCAM ICD (+) as compared to neighboring non-transfected neurons (DSCAM ICD (-) ($^{\#\#}p \leq 0.01$).
(D) Reduced PSD95 density in transfected (DSCAM ICD (+)) and neighboring non-transfected neurons (DSCAM ICD (-)) as compared to control neurons expressing YFP (***$p \leq 0.001$, **$p \leq 0.01$).
(C-D) Bar graphs show mean ± SEM and p-values by ordinary one-way Anova with Turkey's multiple comparisons test.

Figure S8 (related to Figure 6).
(A) Split color channels of MAP2, YFP, PSD95, and VGlut1 immuno-staining shown in Figure 6J and J'.

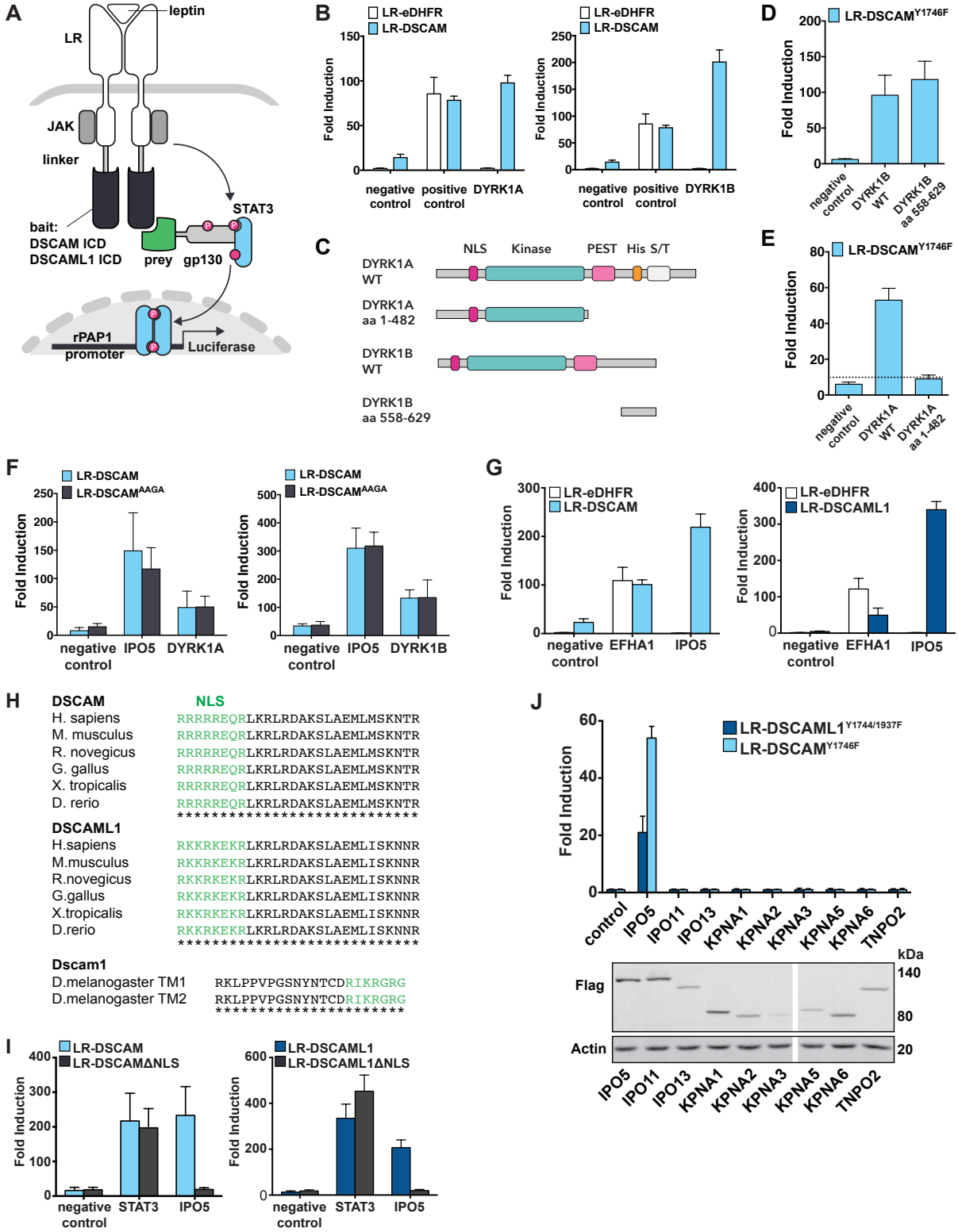
A
leptin
LR
JAK
linker
STAT3
bait:
DSCAM ICD
DSCAML1 ICD
prey
gp130
rPAP1
promoter
Luciferase
B
LR-eDHFR
LR-DSCAM
Fold Induction
negative control
positive control
DYRK1A
DYRK1B
C
NLS
Kinase
PEST
His
S/T
DYRK1A WT
DYRK1A aa 1-482
DYRK1B WT
DYRK1B aa 558-629
D
LR-DSCAM Y1746F
negative control
DYRK1B WT
DYRK1B aa 558-629
E
LR-DSCAM Y1746F
negative control
DYRK1A WT
DYRK1A aa 1-482
F
LR-DSCAM
LR-DSCAM AAGA
negative control
IPO5
DYRK1A
DYRK1B
G
LR-eDHFR
LR-DSCAM
LR-DSCAML1
negative control
EFHA1
IPO5
H
DSCAM
NLS
H. sapiens RRRRREQRLKRLRDAKSLAEMLMSKNTR
M. musculus RRRRREQRLKRLRDAKSLAEMLMSKNTR
R. novegicus RRRRREQRLKRLRDAKSLAEMLMSKNTR
G. gallus RRRRREQRLKRLRDAKSLAEMLMSKNTR
X. tropicalis RRRRREQRLKRLRDAKSLAEMLMSKNTR
D. rerio RRRRREQRLKRLRDAKSLAEMLMSKNTR
DSCAML1
H.sapiens RKKRKEKRLKRLRDAKSLAEMLISKNNR
M.musculus RKKRKEKRLKRLRDAKSLAEMLISKNNR
R.novegicus RKKRKEKRLKRLRDAKSLAEMLISKNNR
G.gallus RKKRKEKRLKRLRDAKSLAEMLISKNNR
X.tropicalis RKKRKEKRLKRLRDAKSLAEMLISKNNR
D.rerio RKKRKEKRLKRLRDAKSLAEMLISKNNR
Dscam1
D.melanogaster TM1 RKLPPVPGSNYNTCDRIKRGRG
D.melanogaster TM2 RKLPPVPGSNYNTCDRIKRGRG
I
LR-DSCAM
LR-DSCAM ΔNLS
LR-DSCAML1
LR-DSCAML1 ΔNLS
negative control
STAT3
IPO5
J
LR-DSCAML1 Y1744/1937F
LR-DSCAM Y1746F
control
IPO5
IPO11
IPO13
KPNA1
KPNA2
KPNA3
KPNA5
KPNA6
TNPO2
kDa
Flag
Actin
140
80
20

Figure 1

Symbol	Name	Function	Interaction with DSCAM	Interaction with DSCAML1
IPO5	Importin 5	Nuclear protein import. Binds to cargo NLS.	Binds to NLS of DSCAM: RRRRREQR (Figure 1G)	Binds to NLS of DSCAML1: RKKRKEKR (Figure 1G)
STAT3	Signal transducer and activator of transcription 3	Transcriptional activator in response to cytokines and growth factors.	Binds to YASQ motif of DSCAM (Figure S2 B)	Binds to YSSQ and YHTQ motif of DSCAML1 (Figure S2 E)
SH2D2A	SH2 domain containing 2A	SH2 domain adaptor protein for VEGF receptor KDR. Functions in T-cell signal transduction.	N/A (figure S2 J)	Binds to YCNL motif of DSCAML1 (figure S2 I)
DYRK1A	Dual-Specificity-Tyrosine-Phosphorylation Regulated Kinase 1A	S/T/Y-kinase. Plays important roles in neuronal development. Down Syndrome candidate gene.	Interaction through C-terminus of DYRK1A (Figure 1E)	Interaction through C-terminus of DYRK1A (Figure S3 B)
DYRK1B	Dual-Specificity-Tyrosine-Phosphorylation Regulated Kinase 1B	S/T/Y-kinase. Regulates transcription in the nucleus.	Interaction through C-terminus of DYRK1B (Figure 1D)	Interaction through C-terminus of DYRK1B (Figure S3 A)
USP21	Ubiquitin specific peptidase 21	Cysteine protease with dual specificity to cleave Ubiquitin and Nedd8.	Binds to YASQ motif of DSCAM (Figure S2 C)	Binds to YSSQ and YHTQ motif of DSCAML1 (Figure S2F)

Table 1

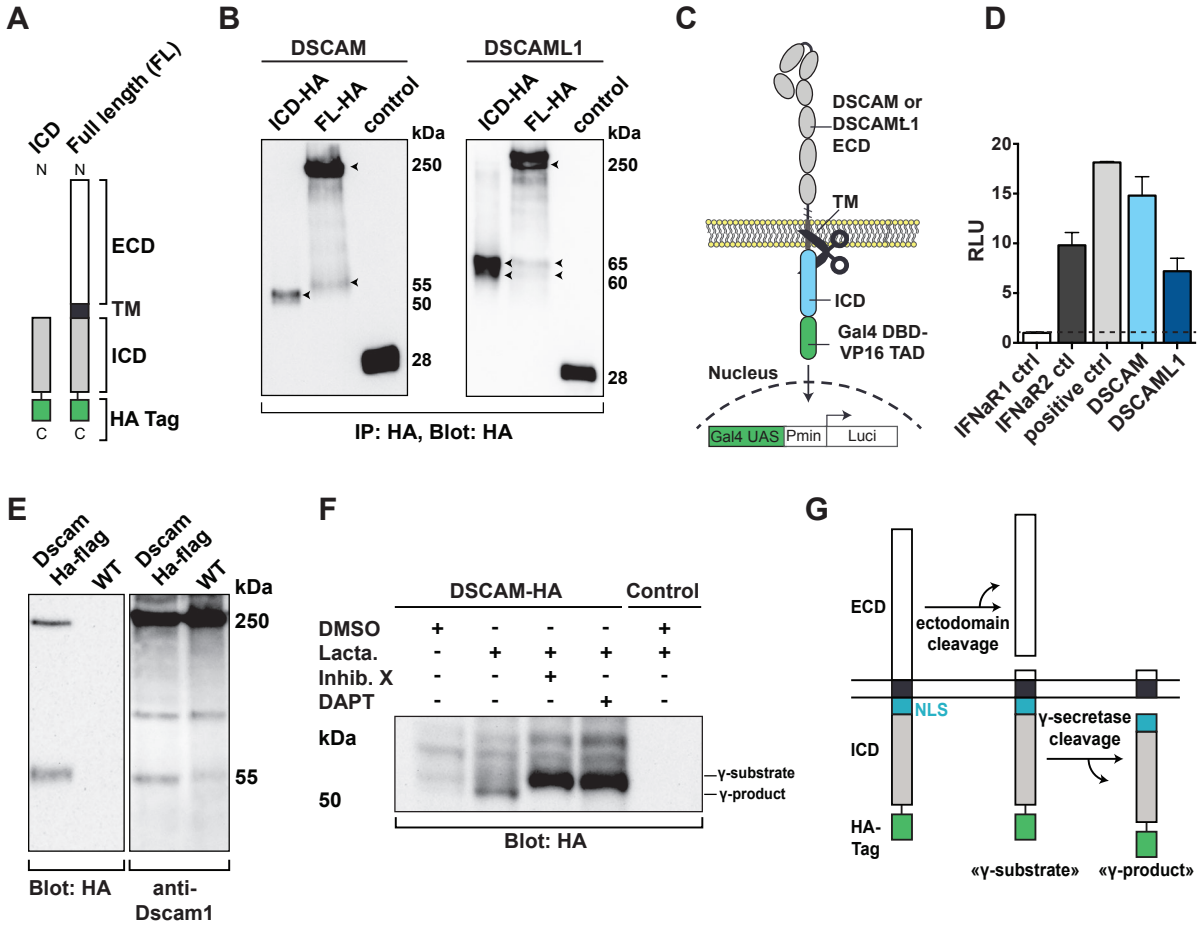
A
ICD
Full length (FL)
N
N
ECD
TM
ICD
HA Tag
C
C
B
DSCAM
DSCAML1
ICD-HA
FL-HA
control
kDa
250
55
50
28
65
60
IP: HA, Blot: HA
C
DSCAM or
DSCAML1
ECD
TM
ICD
Gal4 DBD-
VP16 TAD
Nucleus
Gal4 UAS
Pmin
Luci
D
RLU
20
15
10
5
0
IFNaR1 ctrl
IFNaR2 ctl
positive ctrl
DSCAM
DSCAML1
E
Dscam
Ha-flag
WT
kDa
250
55
Blot: HA
anti-
Dscam1
F
DSCAM-HA
Control
DMSO
Lacta.
Inhib. X
DAPT
kDa
50
γ-substrate
γ-product
Blot: HA
G
ECD
ectodomain
cleavage
NLS
ICD
γ-secretase
cleavage
HA-
Tag
«γ-substrate»
«γ-product»

Figure 2

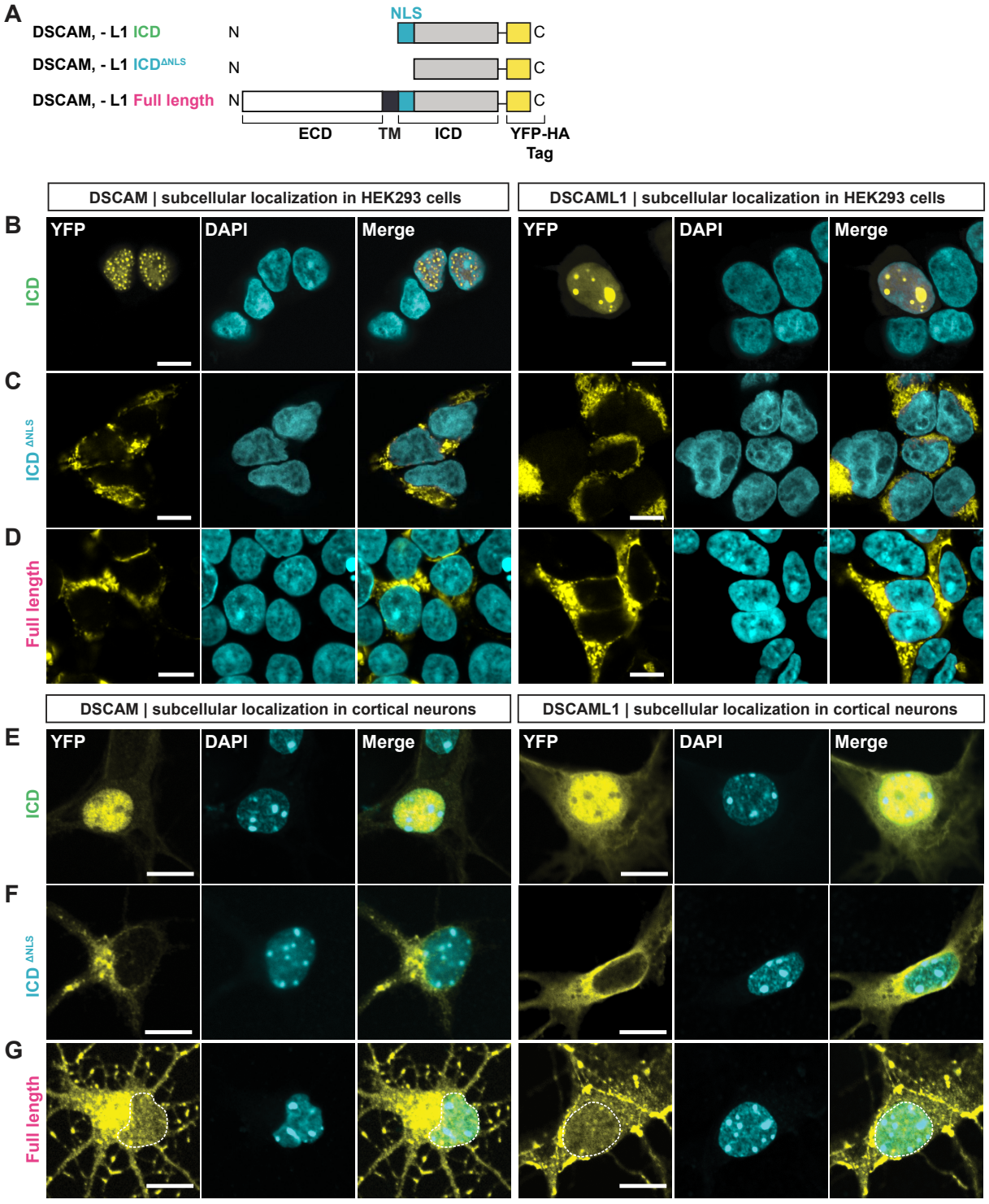
A
DSCAM, - L1 ICD
DSCAM, - L1 ICDΔNLS
DSCAM, - L1 Full length
N
C
NLS
ECD
TM
ICD
YFP-HA Tag
DSCAM | subcellular localization in HEK293 cells
DSCAML1 | subcellular localization in HEK293 cells
B
C
D
YFP
DAPI
Merge
ICD
ICD ΔNLS
Full length
DSCAM | subcellular localization in cortical neurons
DSCAML1 | subcellular localization in cortical neurons
E
F
G

Figure 3

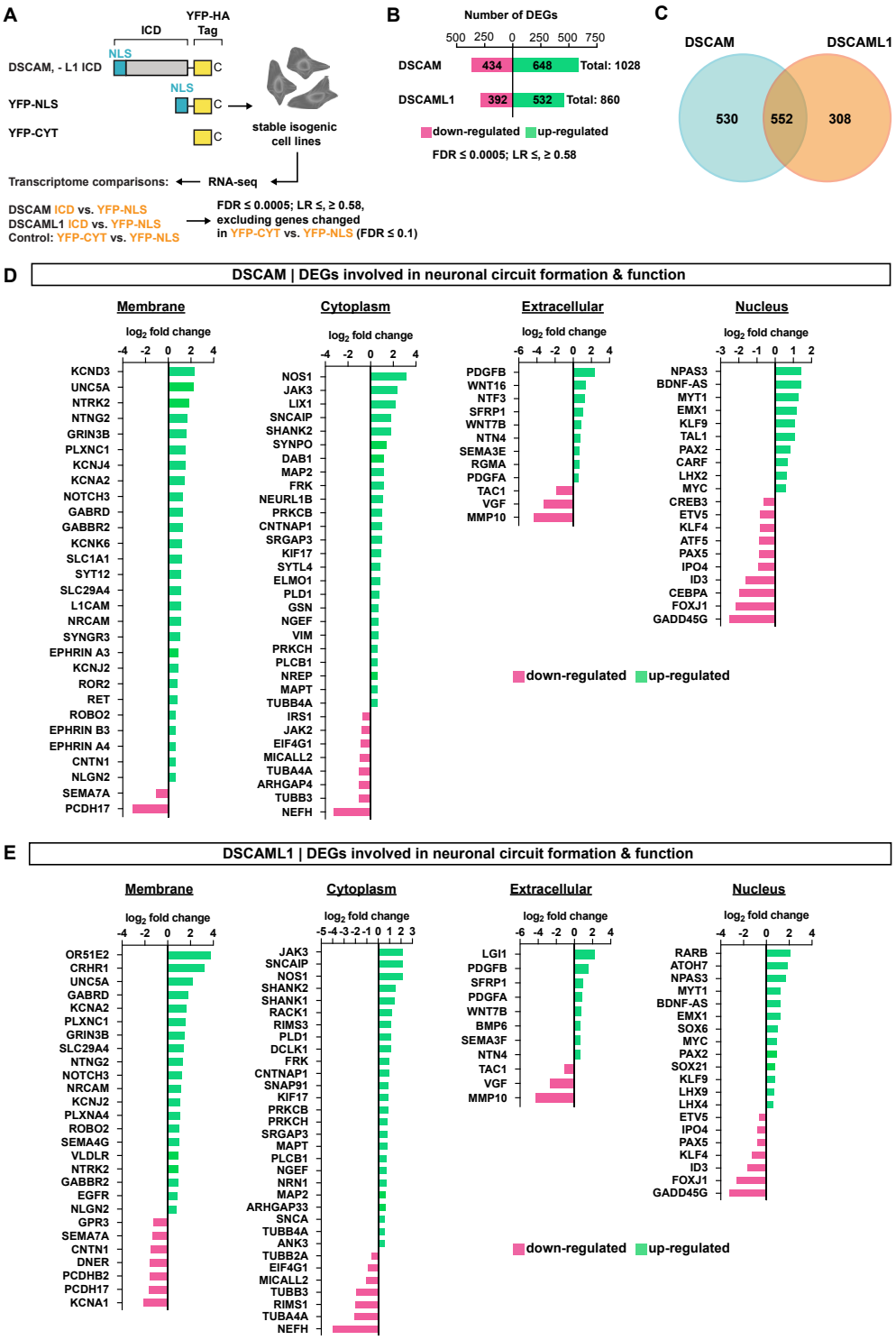
A
ICD
YFP-HA Tag
NLS
DSCAM, - L1 ICD
C
NLS
YFP-NLS
C
YFP-CYT
C
stable isogenic cell lines
Transcriptome comparisons:
RNA-seq
DSCAM ICD vs. YFP-NLS
DSCAML1 ICD vs. YFP-NLS
Control: YFP-CYT vs. YFP-NLS
FDR ≤ 0.0005; LR ≤, ≥ 0.58, excluding genes changed in YFP-CYT vs. YFP-NLS (FDR ≤ 0.1)
B
Number of DEGs
500 250 0 250 500 750
DSCAM
434
648
Total: 1028
DSCAML1
392
532
Total: 860
down-regulated
up-regulated
FDR ≤ 0.0005; LR ≤, ≥ 0.58
C
DSCAM
DSCAML1
530
552
308
D
DSCAM | DEGs involved in neuronal circuit formation & function
Membrane
Cytoplasm
Extracellular
Nucleus
log2 fold change
KCND3
UNC5A
NTRK2
NTNG2
GRIN3B
PLXNC1
KCNJ4
KCNA2
NOTCH3
GABRD
GABBR2
KCNK6
SLC1A1
SYT12
SLC29A4
L1CAM
NRCAM
SYNGR3
EPHRIN A3
KCNJ2
ROR2
RET
ROBO2
EPHRIN B3
EPHRIN A4
CNTN1
NLGN2
SEMA7A
PCDH17
NOS1
JAK3
LIX1
SNCAIP
SHANK2
SYNPO
DAB1
MAP2
FRK
NEURL1B
PRKCB
CNTNAP1
SRGAP3
KIF17
SYTL4
ELMO1
PLD1
GSN
NGEF
VIM
PRKCH
PLCB1
NREP
MAPT
TUBB4A
IRS1
JAK2
EIF4G1
MICALL2
TUBA4A
ARHGAP4
TUBB3
NEFH
PDGFB
WNT16
NTF3
SFRP1
WNT7B
NTN4
SEMA3E
RGMA
PDGFA
TAC1
VGF
MMP10
NPAS3
BDNF-AS
MYT1
EMX1
KLF9
TAL1
PAX2
CARF
LHX2
MYC
CREB3
ETV5
KLF4
ATF5
PAX5
IPO4
ID3
CEBPA
FOXJ1
GADD45G
down-regulated
up-regulated
E
DSCAML1 | DEGs involved in neuronal circuit formation & function
Membrane
Cytoplasm
Extracellular
Nucleus
log2 fold change
OR51E2
CRHR1
UNC5A
GABRD
KCNA2
PLXNC1
GRIN3B
SLC29A4
NTNG2
NOTCH3
NRCAM
KCNJ2
PLXNA4
ROBO2
SEMA4G
VLDLR
NTRK2
GABBR2
EGFR
NLGN2
GPR3
SEMA7A
CNTN1
DNER
PCDHB2
PCDH17
KCNA1
JAK3
SNCAIP
NOS1
SHANK2
SHANK1
RACK1
RIMS3
PLD1
DCLK1
FRK
CNTNAP1
SNAP91
KIF17
PRKCB
PRKCH
SRGAP3
MAPT
PLCB1
NGEF
NRN1
MAP2
ARHGAP33
SNCA
TUBB4A
ANK3
TUBB2A
EIF4G1
MICALL2
TUBB3
RIMS1
TUBA4A
NEFH
LGI1
PDGFB
SFRP1
PDGFA
WNT7B
BMP6
SEMA3F
NTN4
TAC1
VGF
MMP10
RARB
ATOH7
NPAS3
MYT1
BDNF-AS
EMX1
SOX6
MYC
PAX2
SOX21
KLF9
LHX9
LHX4
ETV5
IPO4
PAX5
KLF4
ID3
FOXJ1
GADD45G
down-regulated
up-regulated

Figure 4

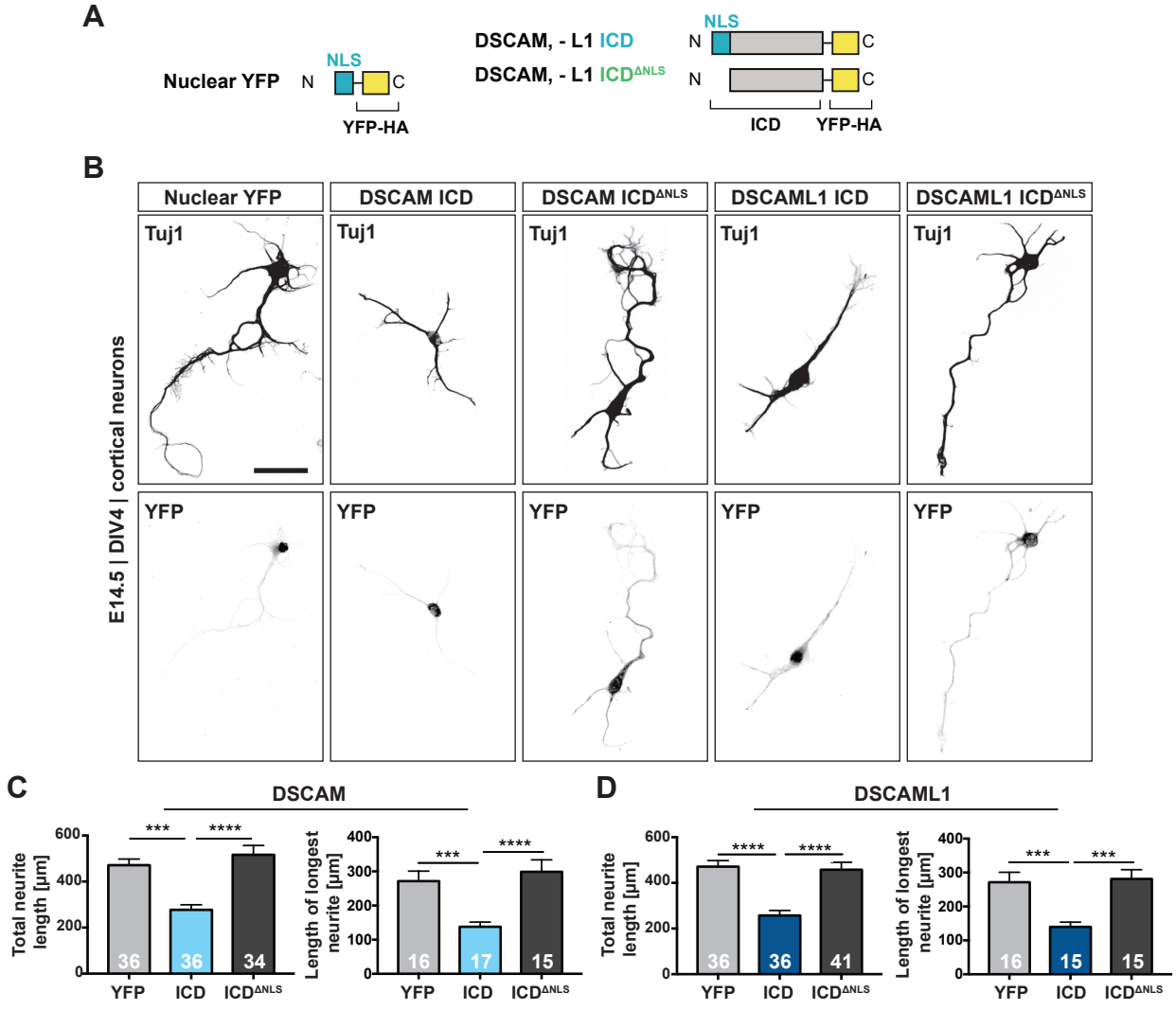
A
Nuclear YFP
N
NLS
C
YFP-HA
DSCAM, - L1 ICD
DSCAM, - L1 ICDΔNLS
N
NLS
C
N
C
ICD
YFP-HA
B
Nuclear YFP
DSCAM ICD
DSCAM ICDΔNLS
DSCAML1 ICD
DSCAML1 ICDΔNLS
E14.5 | DIV4 | cortical neurons
Tuj1
YFP
C
DSCAM
Total neurite length [µm]
Length of longest neurite [µm]
YFP
ICD
ICDΔNLS
36
36
34
16
17
15
D
DSCAML1
36
36
41
16
15
15
***
****

Figure 5

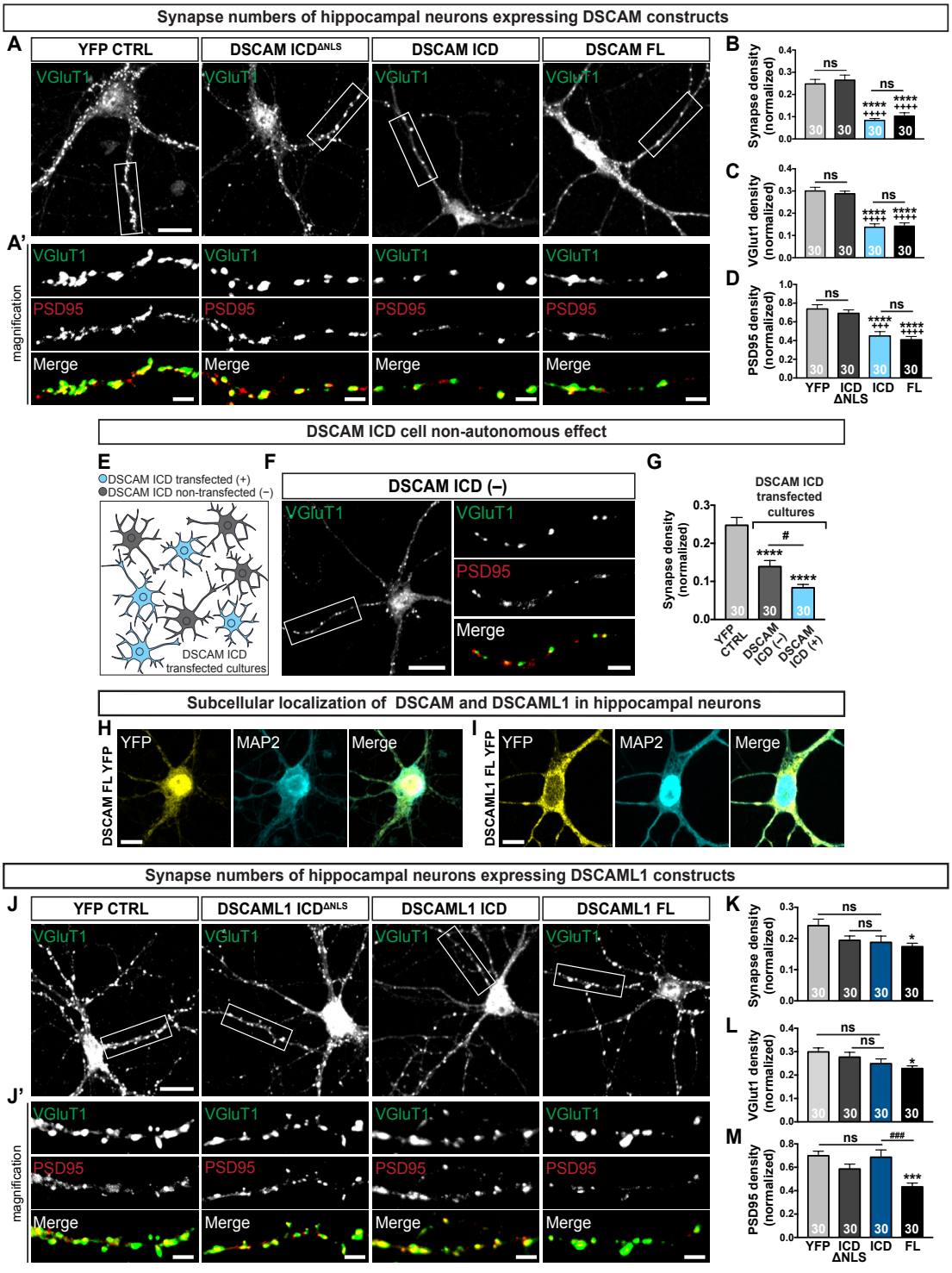
Synapse numbers of hippocampal neurons expressing DSCAM constructs
A
YFP CTRL
DSCAM ICDΔNLS
DSCAM ICD
DSCAM FL
VGluT1
A'
magnification
PSD95
Merge
B
Synapse density (normalized)
C
VGlut1 density (normalized)
D
PSD95 density (normalized)
ns
YFP
ICD ΔNLS
ICD
FL
DSCAM ICD cell non-autonomous effect
E
DSCAM ICD transfected (+)
DSCAM ICD non-transfected (−)
DSCAM ICD transfected cultures
F
DSCAM ICD (–)
G
DSCAM ICD transfected cultures
YFP CTRL
DSCAM ICD (–)
DSCAM ICD (+)
Subcellular localization of DSCAM and DSCAML1 in hippocampal neurons
H
DSCAM FL YFP
YFP
MAP2
Merge
I
DSCAML1 FL YFP
Synapse numbers of hippocampal neurons expressing DSCAML1 constructs
J
YFP CTRL
DSCAML1 ICDΔNLS
DSCAML1 ICD
DSCAML1 FL
J'
magnification
K
Synapse density (normalized)
L
VGlut1 density (normalized)
M
PSD95 density (normalized)

Figure 6

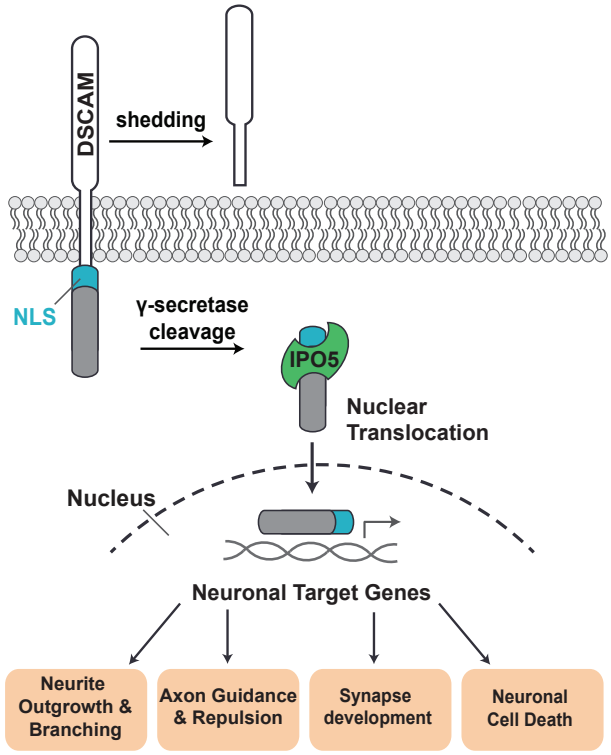
DSCAM
shedding
NLS
γ-secretase
cleavage
IPO5
Nuclear
Translocation
Nucleus
Neuronal Target Genes
Neurite
Outgrowth &
Branching
Axon Guidance
& Repulsion
Synapse
development
Neuronal
Cell Death

Figure 7

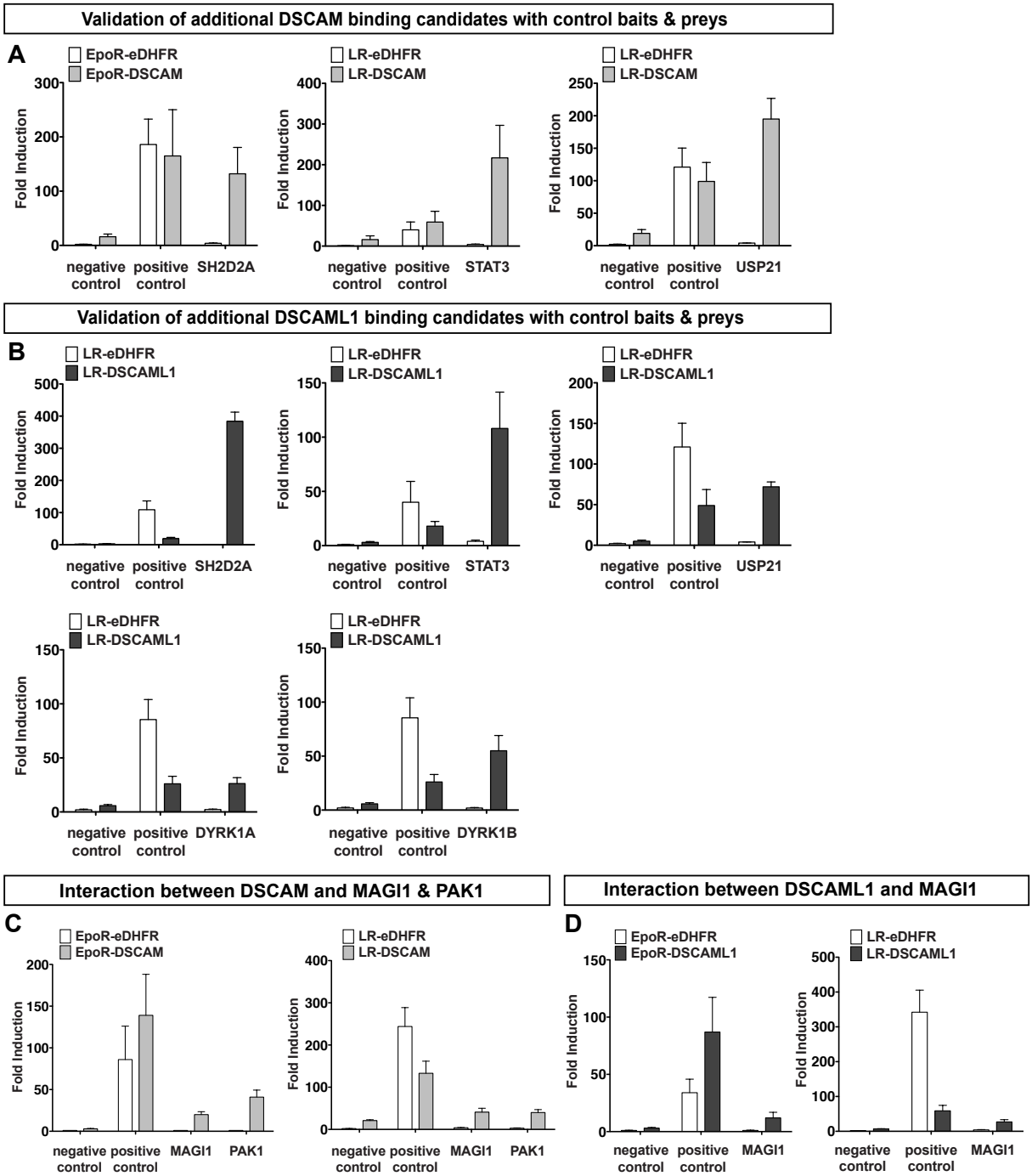
Validation of additional DSCAM binding candidates with control baits & preys
A
EpoR-eDHFR
EpoR-DSCAM
LR-eDHFR
LR-DSCAM
Fold Induction
negative control
positive control
SH2D2A
STAT3
USP21
Validation of additional DSCAML1 binding candidates with control baits & preys
B
LR-eDHFR
LR-DSCAML1
DYRK1A
DYRK1B
Interaction between DSCAM and MAGI1 & PAK1
C
MAGI1
PAK1
Interaction between DSCAML1 and MAGI1
D
EpoR-DSCAML1

Figure S1

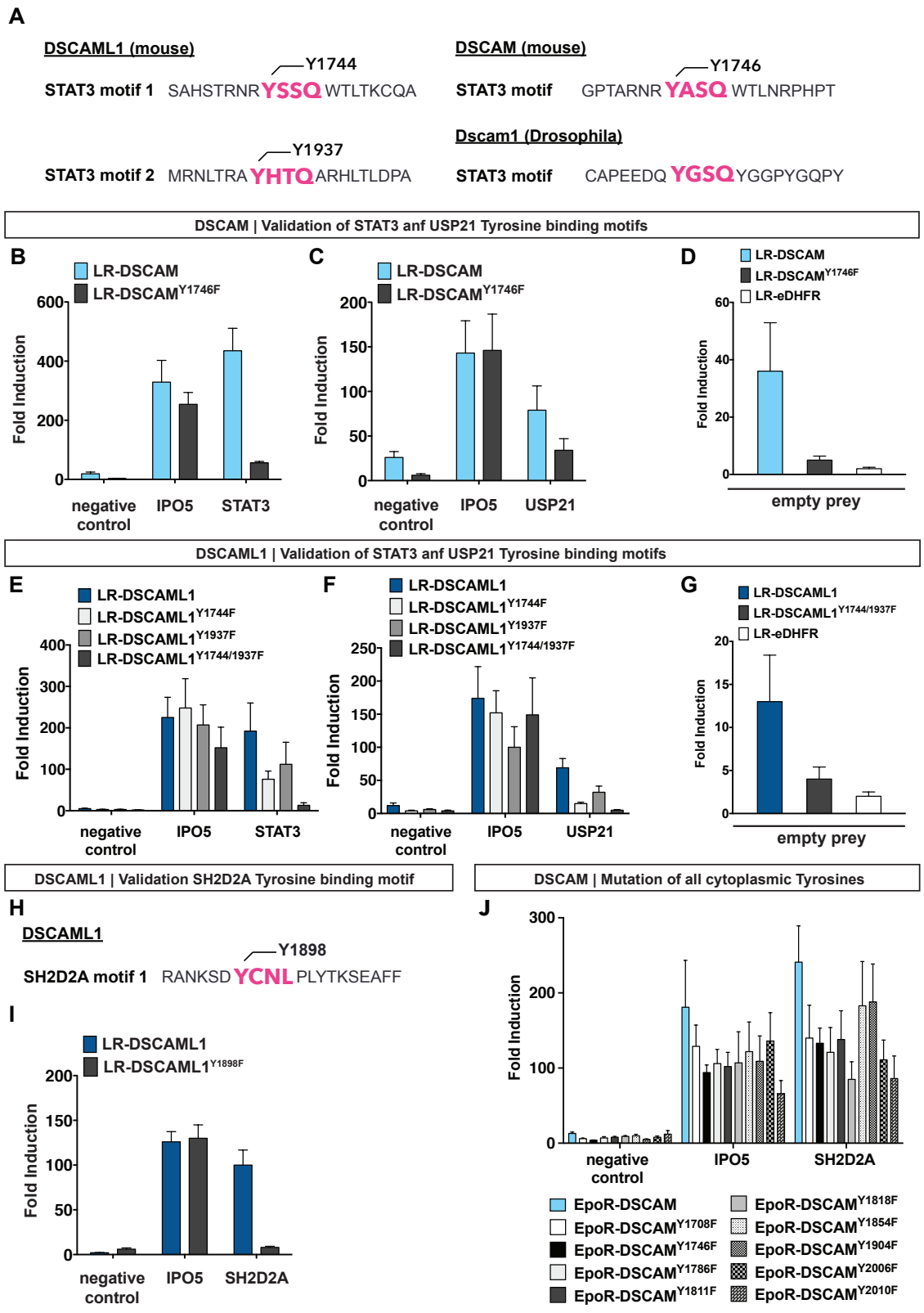
A
DSCAML1 (mouse)
STAT3 motif 1 SAHSTRNRYSSQWTLTKCQA
Y1744
STAT3 motif 2 MRNLTRAYHTQARHLTLDPA
Y1937
DSCAM (mouse)
STAT3 motif GPTARNRYASQWTLNRPHPT
Y1746
Dscam1 (Drosophila)
STAT3 motif CAPEEDQYGSQYGGPYGQPY
DSCAM | Validation of STAT3 anf USP21 Tyrosine binding motifs
B
LR-DSCAM
LR-DSCAMY1746F
Fold Induction
negative control
IPO5
STAT3
C
LR-DSCAM
LR-DSCAMY1746F
Fold Induction
negative control
IPO5
USP21
D
LR-DSCAM
LR-DSCAMY1746F
LR-eDHFR
Fold Induction
empty prey
DSCAML1 | Validation of STAT3 anf USP21 Tyrosine binding motifs
E
LR-DSCAML1
LR-DSCAML1Y1744F
LR-DSCAML1Y1937F
LR-DSCAML1Y1744/1937F
Fold Induction
negative control
IPO5
STAT3
F
LR-DSCAML1
LR-DSCAML1Y1744F
LR-DSCAML1Y1937F
LR-DSCAML1Y1744/1937F
Fold Induction
negative control
IPO5
USP21
G
LR-DSCAML1
LR-DSCAML1Y1744/1937F
LR-eDHFR
Fold Induction
empty prey
DSCAML1 | Validation SH2D2A Tyrosine binding motif
H
DSCAML1
SH2D2A motif 1 RANKSDYCNLPLYTKSEAFF
Y1898
I
LR-DSCAML1
LR-DSCAML1Y1898F
Fold Induction
negative control
IPO5
SH2D2A
DSCAM | Mutation of all cytoplasmic Tyrosines
J
Fold Induction
negative control
IPO5
SH2D2A
EpoR-DSCAM
EpoR-DSCAMY1708F
EpoR-DSCAMY1746F
EpoR-DSCAMY1786F
EpoR-DSCAMY1811F
EpoR-DSCAMY1818F
EpoR-DSCAMY1854F
EpoR-DSCAMY1904F
EpoR-DSCAMY2006F
EpoR-DSCAMY2010F

Figure S2

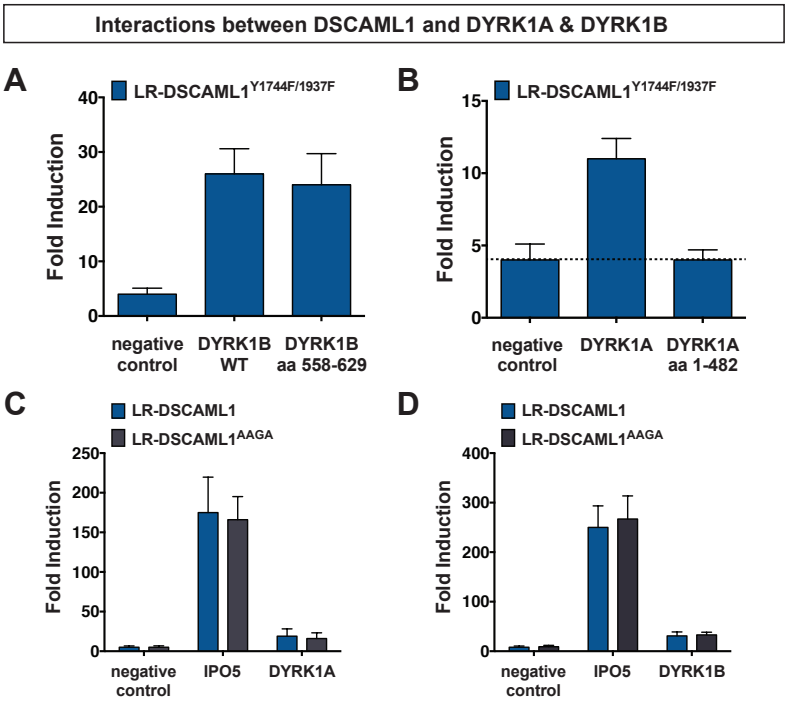
Interactions between DSCAML1 and DYRK1A & DYRK1B
A
LR-DSCAML1Y1744F/1937F
Fold Induction
40
30
20
10
0
negative control
DYRK1B WT
DYRK1B aa 558-629
B
LR-DSCAML1Y1744F/1937F
Fold Induction
15
10
5
0
negative control
DYRK1A
DYRK1A aa 1-482
C
LR-DSCAML1
LR-DSCAML1AAGA
Fold Induction
250
200
150
100
50
0
negative control
IPO5
DYRK1A
D
LR-DSCAML1
LR-DSCAML1AAGA
Fold Induction
400
300
200
100
0
negative control
IPO5
DYRK1B

Figure S3

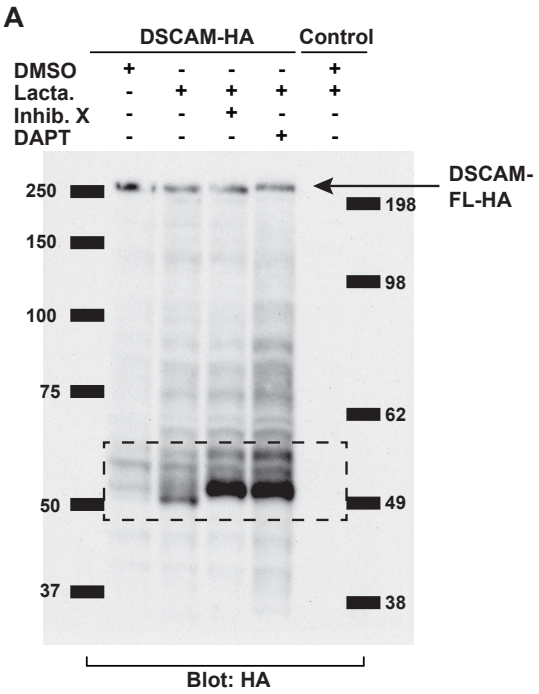
A
DSCAM-HA
Control
DMSO + - - - +
Lacta. - + + + +
Inhib. X - - + - -
DAPT - - - + -
250
150
100
75
50
37
198
98
62
49
38
DSCAM-
FL-HA
Blot: HA

Figure S4

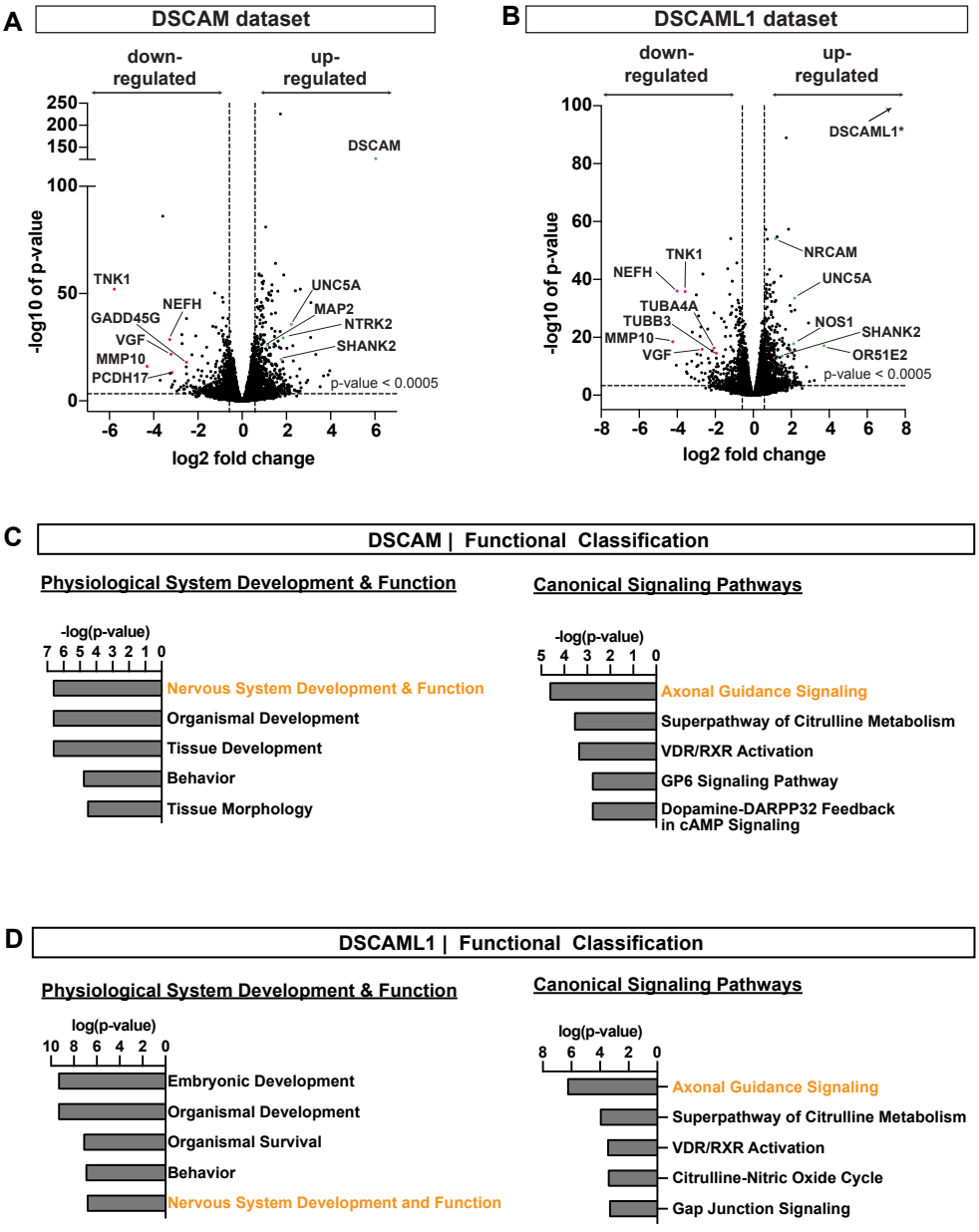
A
DSCAM dataset
down-regulated
up-regulated
-log10 of p-value
log2 fold change
DSCAM
TNK1
NEFH
GADD45G
VGF
MMP10
PCDH17
UNC5A
MAP2
NTRK2
SHANK2
p-value < 0.0005
B
DSCAML1 dataset
DSCAML1*
NRCAM
UNC5A
NOS1
SHANK2
OR51E2
TUBA4A
TUBB3
C
DSCAM | Functional Classification
Physiological System Development & Function
-log(p-value)
Nervous System Development & Function
Organismal Development
Tissue Development
Behavior
Tissue Morphology
Canonical Signaling Pathways
Axonal Guidance Signaling
Superpathway of Citrulline Metabolism
VDR/RXR Activation
GP6 Signaling Pathway
Dopamine-DARPP32 Feedback in cAMP Signaling
D
DSCAML1 | Functional Classification
log(p-value)
Embryonic Development
Organismal Development
Organismal Survival
Behavior
Nervous System Development and Function
Citrulline-Nitric Oxide Cycle
Gap Junction Signaling

Figure S5

Symbol	Entrez Gene Name	Log2 fold change	FDR
PDGFB	platelet derived growth factor subunit B	2,314	2,64E-19
UNC5A	unc-5 netrin receptor A	2,221	1,69E-36
PAPPA	pappalysin 1	1,904	3,54E-13
NTRK2	neurotrophic receptor tyrosine kinase 2	1,858	5,03E-30
SHANK2	SH3 and multiple ankyrin repeat domains 2	1,771	5,01E-20
NTNG2	netrin G2	1,717	3,30E-15
PLXNC1	plexin C1	1,535	1,11E-17
WNT16	Wnt family member 16	1,334	1,01E-09
RRAS	related RAS viral (r-ras) oncogene homolog	1,330	3,65E-06
NTF3	neurotrophin 3	1,240	3,43E-04
L1CAM	L1 cell adhesion molecule	1,104	1,17E-07
PRKCB	protein kinase C beta	1,020	1,78E-31
GNG7	G protein subunit gamma 7	0,986	1,39E-11
SRGAP3	SLIT-ROBO Rho GTPase activating protein 3	0,972	1,22E-12
EFNA3	ephrin A3	0,906	4,85E-09
WNT7B	Wnt family member 7B	0,854	4,37E-07
NFAT5	nuclear factor of activated T-cells 5	0,813	3,94E-12
NTN4	netrin 4	0,798	2,58E-11
ADAMTS9	ADAM metallopeptidase with thrombospondin type 1 motif 9	0,742	7,19E-06
ROBO2	roundabout guidance receptor 2	0,693	9,36E-12
EFNB3	ephrin B3	0,686	2,88E-09
PIK3C2B	phosphatidylinositol-4-phosphate 3-kinase catalytic subunit type 2 beta	0,677	3,28E-12
EFNA4	ephrin A4	0,670	3,31E-04
NGEF	neuronal guanine nucleotide exchange factor	0,663	1,49E-07
GNAO1	G protein subunit alpha o1	0,663	1,34E-09
SEMA3E	semaphorin 3E	0,636	1,08E-09
PRKCH	protein kinase C eta	0,623	2,56E-10
PLCB1	phospholipase C beta 1	0,616	5,87E-12
TUBB4A	tubulin beta 4A class IVa	0,596	5,58E-07
PDGFA	platelet derived growth factor subunit A	0,589	1,53E-05
RGS3	regulator of G protein signaling 3	0,587	2,36E-11
IRS1	insulin receptor substrate 1	-0,686	8,42E-12
ECE2	endothelin converting enzyme 2	-0,864	3,25E-13
RTN4R	reticulon 4 receptor	-0,996	2,98E-09
TUBA4A	tubulin alpha 4a	-1,020	1,19E-06
SEMA7A	semaphorin 7A (John Milton Hagen blood group)	-1,031	2,38E-04
TUBB3	tubulin beta 3 class III	-1,036	7,73E-07
ADAMTS4	ADAM metallopeptidase with thrombospondin type 1 motif 4	-1,681	2,46E-05
MMP10	matrix metallopeptidase 10	-4,304	8,20E-17

Table S1

Symbol	Entrez Gene Name	Log2 fold change	FDR
UNC5A	unc-5 netrin receptor A	2,180	2,68E-34
WNT4	Wnt family member 4	2,170	1,52E-07
NOTUM	NOTUM, palmitoleoyl-protein carboxylesterase	1,901	2,16E-04
PLXNC1	plexin C1	1,567	5,81E-18
PDGFB	platelet derived growth factor subunit B	1,549	7,11E-08
SHANK2	SH3 and multiple ankyrin repeat domains 2	1,522	2,84E-14
NTNG2	netrin G2	1,292	1,68E-08
RACK1	receptor for activated C kinase 1	1,246	2,10E-09
PLCB2	phospholipase C beta 2	1,232	2,05E-04
GNG7	G protein subunit gamma 7	1,125	1,09E-14
ADAMTS9	ADAM metallopeptidase with thrombospondin type 1 motif 9	1,053	5,71E-11
ROBO2	roundabout guidance receptor 2	1,011	1,20E-24
SEMA4G	semaphorin 4G	0,986	6,39E-06
PIK3CD	phosphatidylinositol-4,5-bisphosphate 3-kinase catalytic subunit delta	0,959	1,59E-06
NTRK2	neurotrophic receptor tyrosine kinase 2	0,912	8,45E-07
PRKCB	protein kinase C beta	0,854	7,10E-22
GDF7	growth differentiation factor 7	0,830	4,07E-09
PDGFA	platelet derived growth factor subunit A	0,826	4,84E-10
PRKCH	protein kinase C eta	0,793	5,22E-16
SRGAP3	SLIT-ROBO Rho GTPase activating protein 3	0,785	2,69E-08
WNT7B	Wnt family member 7B	0,759	1,19E-05
PLCB1	phospholipase C beta 1	0,724	3,93E-16
NGEF	neuronal guanine nucleotide exchange factor	0,714	1,88E-08
BMP6	bone morphogenetic protein 6	0,687	5,57E-10
GNAZ	G protein subunit alpha z	0,685	2,67E-26
DPYSL5	dihydropyrimidinase like 5	0,662	5,83E-58
GNAO1	G protein subunit alpha o1	0,659	2,38E-09
SEMA3F	semaphorin 3F	0,652	1,11E-05
NTN4	netrin 4	0,636	3,46E-07
NFAT5	nuclear factor of activated T-cells 5	0,621	1,85E-07
TUBB4A	tubulin beta 4A class IVa	0,607	3,96E-07
ADAM23	ADAM metallopeptidase domain 23	0,592	9,32E-18
TUBB2A	tubulin beta 2A class IIa	-0,626	3,42E-13
SEMA7A	semaphorin 7A (John Milton Hagen blood group)	-1,337	3,32E-06
PAPPA	pappalysin 1	-1,817	1,20E-05
TUBB3	tubulin beta 3 class III	-1,943	2,84E-15
TUBA4A	tubulin alpha 4a	-2,056	5,31E-17
MMP10	matrix metallopeptidase 10	-4,235	3,07E-19

Table S2

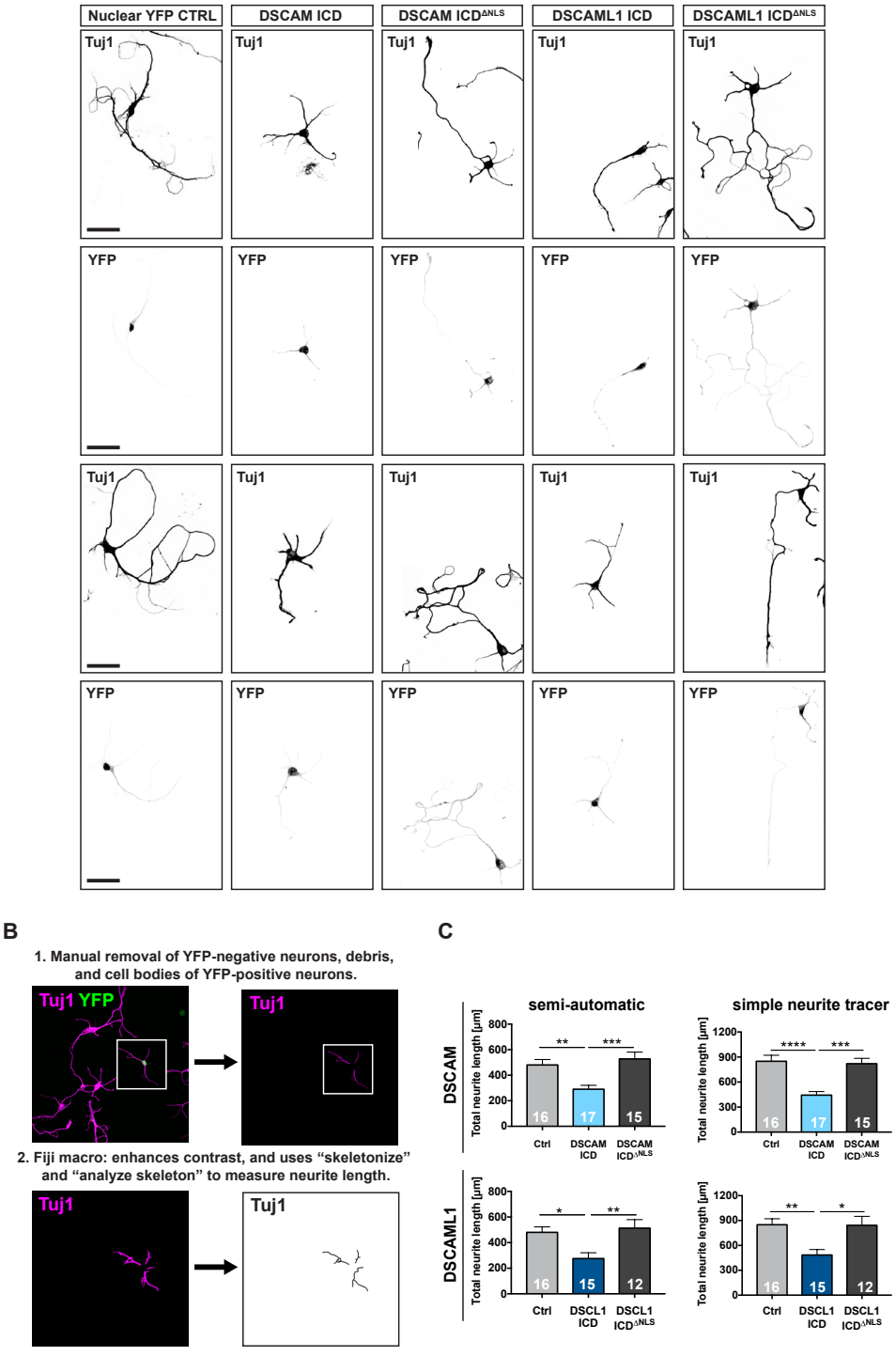
Nuclear YFP CTRL
DSCAM ICD
DSCAM ICDΔNLS
DSCAML1 ICD
DSCAML1 ICDΔNLS
Tuj1
YFP
B
1. Manual removal of YFP-negative neurons, debris, and cell bodies of YFP-positive neurons.
Tuj1 YFP
Tuj1
2. Fiji macro: enhances contrast, and uses "skeletonize" and "analyze skeleton" to measure neurite length.
Tuj1
Tuj1
C
semi-automatic
simple neurite tracer
DSCAM
DSCAML1
Total neurite length [µm]
Ctrl
DSCAM ICD
DSCAM ICDΔNLS
DSCL1 ICD
DSCL1 ICDΔNLS

Figure S6

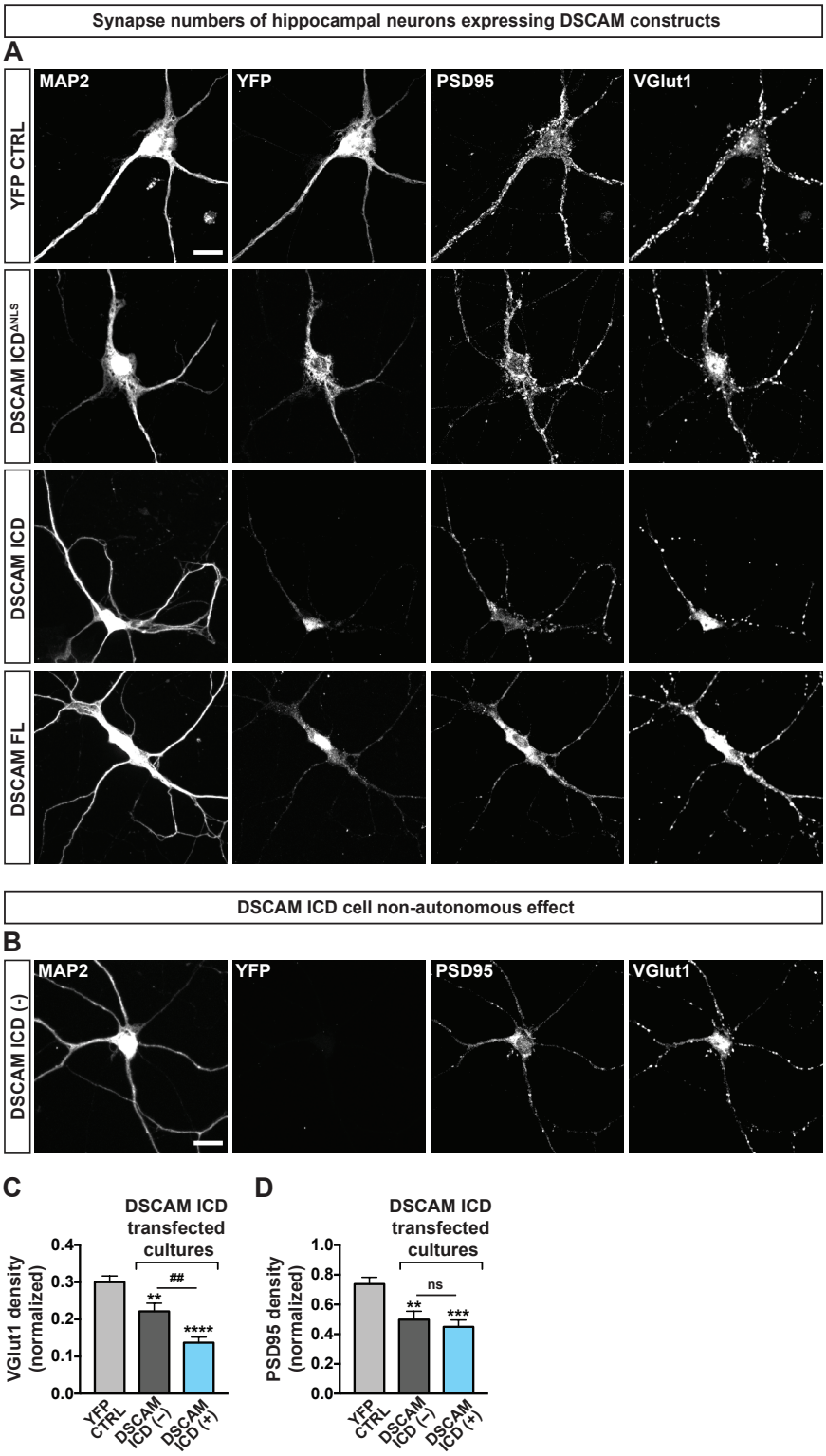
Synapse numbers of hippocampal neurons expressing DSCAM constructs
A
MAP2
YFP
PSD95
VGlut1
YFP CTRL
DSCAM ICD^ΔNLS
DSCAM ICD
DSCAM FL
DSCAM ICD cell non-autonomous effect
B
DSCAM ICD (-)
C
DSCAM ICD transfected cultures
VGlut1 density (normalized)
0.4
0.3
0.2
0.1
0.0
##
**
****
YFP CTRL
DSCAM ICD (–)
DSCAM ICD (+)
D
DSCAM ICD transfected cultures
PSD95 density (normalized)
1.0
0.8
0.6
0.4
0.2
0.0
ns
**
***
YFP CTRL
DSCAM ICD (–)
DSCAM ICD (+)

Figure S7

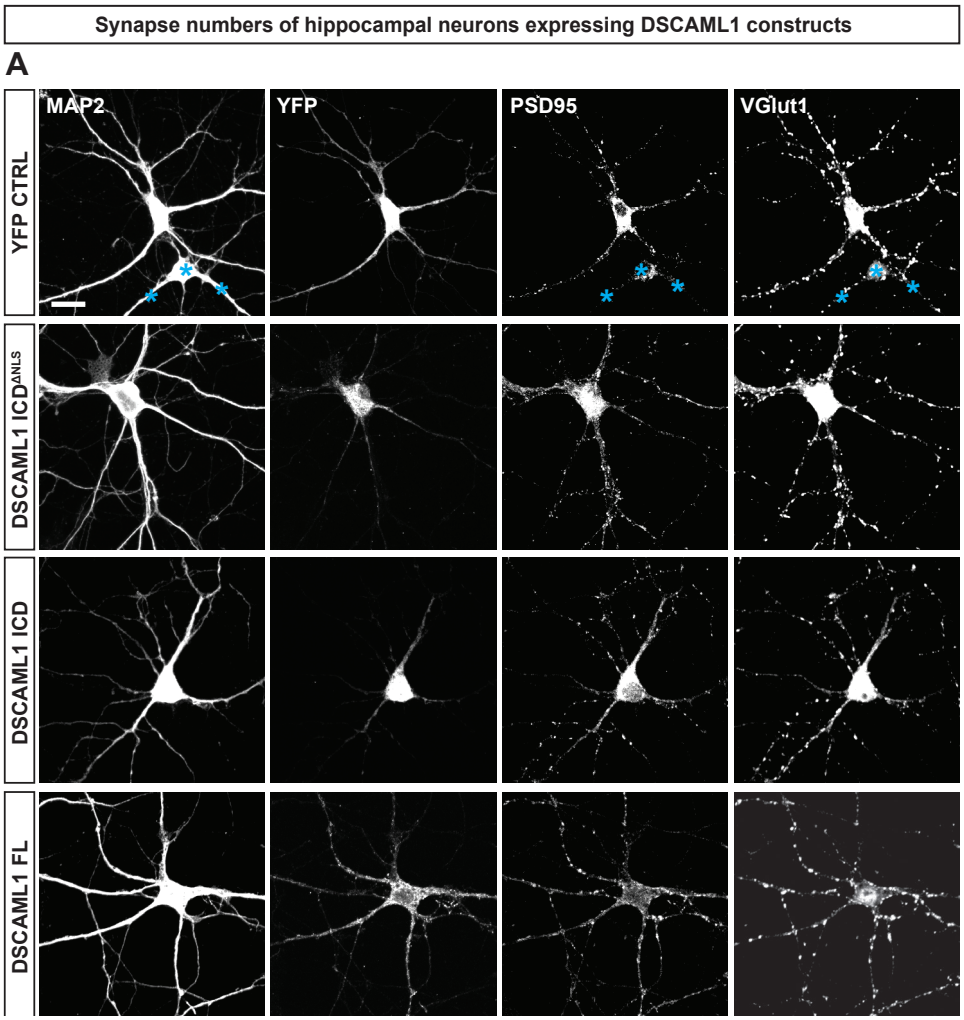
Synapse numbers of hippocampal neurons expressing DSCAML1 constructs
A
MAP2
YFP
PSD95
VGlut1
YFP CTRL
DSCAML1 ICD$^{\Delta NLS}$
DSCAML1 ICD
DSCAML1 FL

Figure S8